https://doi.org/10.5194/acp-2021-917
Preprint. Discussion started: 15 December 2021

Atmospheric Chemistry and Physics Discussions

Examination of aerosol impacts on convective clouds and precipitation in two metropolitan areas in East Asia; how varying depths of convective clouds between the areas diversify those aerosol effects?

Seoung Soo Lee[1,2], Jinho Choi[3], Goun Kim[4], Kyung-Ja Ha[2,5,6], Kyong-Hwan Seo[3], Junshik Um[3], Youtong Zheng[7]

[1]Earth System Science Interdisciplinary Center, University of Maryland, Maryland

[2]Research Center for Climate Sciences, Pusan National University, Busan, Republic of Korea

[3]Department of Atmospheric Sciences, Division of Earth Environmental System, Pusan National University, Busan, Republic of Korea

[4]Marine Disaster Research Center, Korea Institute of Ocean Science and Technology, Pusan, Republic of Korea

[5]Center for Climate Physics, Institute for Basic Science, Busan, Republic of Korea

[6]BK21 School of Earth and Environmental Systems, Pusan National University, Busan, Republic of Korea

[7]The Program in Atmospheric and Oceanic Sciences, Princeton University, and National Oceanic and Atmospheric Administration/Geophysical Fluid Dynamics Laboratory, Princeton, New Jersey, USA

Corresponding author: Seoung Soo Lee
Office: (303) 497-6615
Fax: (303) 497-5318
E-mail: cumulss@gmail.com, slee1247@umd.edu

https://doi.org/10.5194/acp-2021-917
Preprint. Discussion started: 15 December 2021

Atmospheric Chemistry and Physics Discussions

Abstract

This study examines the role played by aerosols in the development of clouds and precipitation in two metropolitan areas in East Asia that has experienced substantial increases in aerosol concentrations over the last decades. These two areas are the Seoul and Beijing areas and the examination has been done by performing simulations using a cloud-system resolving model (CSRM). Aerosols are advected from the continent to the Seoul area and this increases aerosol concentrations in the Seoul area. These increased aerosol concentrations induce the enhancement of condensation that in turn induces the enhancement of deposition and precipitation amount in a system of less deep convective clouds as compared to those in the Beijing area. In a system of deeper clouds in the Beijing area, increasing aerosol concentrations also enhance condensation but reduce deposition. This leads to aerosol-induced negligible changes in precipitation amount. Also, in the system, there is a competition for convective energy among clouds with different condensation and updrafts. This competition results in different responses to increasing aerosol concentrations among different types of precipitation, which are light, medium and heavy precipitation in the Beijing area. In both of the areas, aerosol-induced changes in freezing play a negligible role in aerosol-precipitation interactions as compared to the role played by aerosol-induced changes in condensation and deposition.

https://doi.org/10.5194/acp-2021-917
Preprint. Discussion started: 15 December 2021


Atmospheric Chemistry and Physics Discussions

1. Introduction

With increasing aerosol loading or concentrations, cloud-particle sizes and autoconversion, which represent cloud microphysical properties, can be changed. Autoconversion is a process where cloud-liquid particles or droplets grow to form raindrops via collision and collection among droplets. In general, with increasing particle sizes, the efficiency of collision and collection among droplets increases. Increasing aerosol loading is known to make the particle size smaller and thus make the efficiency of collision, collection and autoconversion lower. This leads to less cloud liquid which can grow to be raindrops and there is more cloud liquid present in the air to be evaporated or frozen. Studies have shown that increases in cloud-liquid mass due to increasing aerosol loading can enhance the freezing of cloud liquid and parcel buoyancy, which lead to the invigoration of convection (Rosenfeld et al., 2008; Fan et al., 2009). Via the invigoration of convection, precipitation can be enhanced. The dependence of aerosol-induced invigoration of convection and precipitation enhancement on aerosol-induced increases in condensational heating in the warm sector of a cloud system has been shown (e.g., van den Heever et al., 2006; Fan et al., 2009; Lee et al., 2018). Increasing cloud-liquid mass induces increasing evaporation, which intensifies gust fronts. This in turn strengthens convective clouds and increases the amount of precipitation (Khain et al., 2005; Tao et al., 2007; Storer et al., 2010; Tao et al., 2012; Lee et al., 2017; Lee et al., 2018). It is notable that aerosol-induced precipitation enhancement is strongly sensitive to cloud types that can be defined by cloud characteristics such as cloud depth (e.g., Tao et al., 2007; Lee et al., 2008; Fan et al., 2009).

Since East Asia was industrialized, there have been substantial increases in aerosol concentrations over the last decades in East Asia (e.g., Lee et al., 2013; Lu et al., 2011; Oh et al., 2015; Dong et al., 2019). These increases are far greater than those in other regions such as North America and Europe (e.g., Lu et al., 2011; Dong et al., 2019). While those increasing aerosols affect clouds, precipitation and hydrologic circulations in the continental East Asia, the increase in the advected aerosols from the continent to the Korean Peninsula affect clouds, precipitation and hydrologic circulations in the Korean Peninsula (Kar et al., 2009). This study aims to examine effects of the increasing aerosols and their advection on clouds and precipitation in East Asia. As a first step to this

https://doi.org/10.5194/acp-2021-917
Preprint. Discussion started: 15 December 2021


Atmospheric Chemistry and Physics Discussions

examination, this study focuses on two metropolitan areas in East Asia which are the Beijing and Seoul areas. The population of each of the Beijing and Seoul areas is ~ 20 millions. Associated with this, these areas have lots of aerosol sources (e.g., traffic) and have made a substantial contribution to the increases in aerosol concentrations in East Asia. Hence, we believe that these two cities can represent overall situations related to increasing aerosol concentrations in East Asia.

As mentioned above, aerosol-cloud interactions (and their impacts on precipitation) are strongly dependent on cloud types and thus to gain a more general understanding of those interactions, we select cases from the Beijing and Seoul areas with different cloud types. A selected case from the Beijing area involves deep convective clouds that reach the tropopause, while a selected case from the Seoul area involves comparatively shallow (or less deep) convective clouds. Via comparisons between these two cases, we aim to identify mechanisms that control varying aerosol-cloud interactions with cloud types.

To examine impacts of aerosols on clouds and precipitation in the cases, numerical simulations are performed, as a way of fulfilling above-described aim. These simulations use a cloud-system resolving model (CSRM) that has reasonably high resolutions to resolve cloud-scale processes that are related to cloud microphysics and dynamics. Hence, these simulations are able to find process-level mechanisms in association with cloud-scale processes.

2. Case description

In the Seoul area, South Korea, there is an observed mesoscale convective system (MCS) for a period from 03:00 LST (local solar time) to 18:00 LST December 24th 2017. During this period, there is a recorded moderate amount of precipitation and its maximum precipitation rate reaches ~ 13 mm hr^{-1}. At 21:00 LST December 23rd 2017, synoptic-scale features develop in favor of the formation and development of the selected MCS and associated moderate rainfall. A low-pressure trough was over northeast China and the Yellow Sea (Figure 1a). Along the flank of the low-pressure system, there was the southwesterly low-level jets to transport warm and moist air. This warm and moist air is originated from the Yellow Sea and transported to the Korean Peninsula (Figure 1a). The

https://doi.org/10.5194/acp-2021-917
Preprint. Discussion started: 15 December 2021


Atmospheric Chemistry and Physics Discussions

119 southwesterly low-level jet plays an important role in the formation and development of
120 rainfall events in the Korean Peninsula by fetching warm and moist air (Hwang and Lee
121 1993; Lee et al. 1998; Seo et al. 2013; Oh et al. 2018).
122 There was another observed MCS case in the Beijing area, China for a period from
123 14:00 LST on July 27th to 00:00 LST July 28th 2015. There is a substantial recorded amount
124 of precipitation for this period and its maximum precipitation rate reaches ~ 45 mm hr^{-1}.
125 At 09:00 LST July 27th 2015, synoptic-scale features develop in favor of the formation and
126 development of the selected MCS. The southerly low-level jet forms and develops heavy
127 rainfall events in the Beijing area by transporting warm and moist air to the area (Figure
128 1b).
129
130 **3. CSRM and simulations**
131
132 **3.1 CSRM**
133
134 The Advanced Research Weather Research and Forecasting (ARW) model (version 3.3.1)
135 is used as a CSRM. The ARW model is a compressible model with a nonhydrostatic status.
136 A 5th-order monotonic advection scheme is used to advect microphysical variables (Wang
137 et al., 2009). The Rapid Radiation Transfer Model (RRTMG; Mlawer et al., 1997; Fouquart
138 and Bonnel, 1980) is adopted to parameterize shortwave and longwave radiation in
139 simulations. A microphysics scheme that is used in this study calculates the effective sizes
140 of hydrometeors that are fed into the RRTMG, and the RRTMG simulates how these
141 effective sizes affect radiation.
142 The CSRM adopts a bin scheme as a way of parameterizing microphysics. The
143 Hebrew University Cloud Model (HUCM) detailed in Khain et al. (2011) is the bin scheme.
144 A set of kinetic equations is solved by the bin scheme to represent size distribution
145 functions for each class of hydrometeors and aerosols acting as cloud condensation nuclei
146 (CCN). The hydrometeor classes are water drops, ice crystals (plate, columnar and branch
147 types), snow aggregates, graupel and hail. There are 33 bins for each size distribution in a
148 way that the mass of a particle m_j in the j bin is to be $m_j = 2m_{j-1}$.
149

https://doi.org/10.5194/acp-2021-917
Preprint. Discussion started: 15 December 2021


Atmospheric Chemistry and Physics Discussions

3.2 Control runs

For a three-dimensional CSRM simulation of the observed case of convective clouds in the Seoul (Beijing) area, i.e., the control-s (control-b) run, a domain just over the Seoul (Beijing) area, which is shown in Figure 2a (2b), is used. This domain adopts a 300-m resolution. The control-s run is for a period from 03:00 to18:00 LST December 24th 2017, while the control-b run is for a period from 14:00 LST on July 27th to 00:00 LST July 28th 2015. The length of the domain is 170 (140) km in the east-west (north-south) direction for the control-s run, and 280 (240) km for the control-b run. There are 100 vertical layers and these layers employ a sigma coordinate that follows the terrain. The top pressure of the model is 50 hPa for both of the control-s and control-b runs. On average, the vertical resolution is ~200 m.

Reanalysis data, which represent the synoptic-scale features, provide initial and boundary conditions of variables such as wind, potential temperature, and specific humidity for the simulations. The Met Office Unified Model (Brown et al., 2012) produces these data every 6 hours with a 0.11° × 0.11° resolution. The simulations adopt an open lateral boundary condition. The Noah land surface model (LSM; Chen and Dudhia, 2001) calculates surface heat fluxes.

The current version of the ARW model is not able to consider the spatiotemporal variation of aerosol properties. In order to take into account the spatiotemporal variation of aerosol properties, which is typical in metropolitan areas, such as composition and number concentration, an aerosol preprocessor, which is able to consider the variability of aerosol properties, is developed and used in the simulations. This aerosol preprocessor interpolates or extrapolates background aerosol properties in observation data such as aerosol mass (e.g., $PM_{2.5}$ and PM_{10}) into grid points and time steps in the model. PM stands for particulate matter. The mass of aerosols with diameter smaller than 2.5 (10.0) μm per unit volume of the air is $PM_{2.5}$ (PM_{10}).

$PM_{2.5}$ or PM_{10}, which are measured by surface observation sites in the domains, is used to consider the variability of aerosol properties. Here, it is assumed that the mass of aerosols that act as CCN is represented by $PM_{2.5}$ and PM_{10} for the Seoul and Beijing areas, respectively. The distance between the observation sites is ~ 1 km and the time interval

https://doi.org/10.5194/acp-2021-917
Preprint. Discussion started: 15 December 2021


Atmospheric Chemistry and Physics Discussions

between observations of aerosol mass is ~ 10 minutes. Hence, the variability is represented by fine spatiotemporal resolutions of the sites. The ground sites that are equipped with the aerosol robotic network (AERONET; Holben et al., 2001) are in the domains. Distances between these sites are ~10 km. In this study, $PM_{2.5}$/PM_{10} data are used to represent the spatiotemporal variability of aerosols acting as CCN over the domains and the simulation periods. To represent aerosol composition and size distributions, data from the AERONET sites are employed.

For the period with the observed clouds, based on the AERONET data, it is assumed that on average, aerosol particles are internally mixed with 70 (80) % ammonium sulfate and 30 (20) % organic compound for the Seoul (Beijing) case. This mixture is assumed to represent aerosol chemical composition in the whole domain and during the entire simulation period, based on the fact that aerosol composition does not vary significantly over the domain and during the whole period with the observed clouds. Aerosols reflect, scatter and absorb shortwave and longwave radiation before they are activated. This type of aerosol-radiation interactions is not taken into account in this study. This is mainly based on the fact that in the mixture, there is insignificant amount of radiation absorbers; black carbon is a representative radiation absorbers. The AERONET observation indicates that the size distribution of background aerosols acting as CCN follows the tri-modal log-normal distribution for the Seoul (Beijing) case as exemplified in Figure 3a (3b). Hence, it is assumed that for the whole domain and simulation period, the size distribution of background aerosols acting as CCN follows the shape of distribution with specific size distribution parameters (i.e., modal radius and standard deviation of each of nuclei, accumulation and coarse modes, and the partition of aerosol number among those modes) as shown in Figure 3a (3b) for the Seoul (Beijing) case. The assumed shape of the size distribution of background aerosols in Figure 3a (3b) is with the average of the distribution parameters over the AERONET sites and the period with clouds for the Seoul (Beijing) case. Since the AERONET observation shows that the shape of the size distribution does not vary significantly over the domain and during the simulation period for each of the Seoul and Beijing cases, we believe that the assumption is reasonable. By using $PM_{2.5}$ and PM_{10} and based on the assumption of aerosol composition and size distribution above, the background number concentrations of aerosols acting as CCN are obtained. These

https://doi.org/10.5194/acp-2021-917
Preprint. Discussion started: 15 December 2021


Atmospheric Chemistry and Physics Discussions

background number concentrations, associated aerosol size distribution and composition are interpolated or extrapolated to grid points immediately above the surface and time steps in the simulation for each of the cases. There is no variation with height in background aerosol concentrations from immediately above the surface to the top of the planetary boundary layer (PBL). However, it is assumed that they decrease exponentially with height from the PBL top upward. Aerosol size distribution and composition do not vary with height. Once background aerosol properties (i.e., aerosol number concentrations, size distribution and composition) are put into each grid point and time step, those properties at each grid point and time step do not change during the course of the simulations.

For the control-s and control-b runs, aerosol properties of ice-nucleating particles (INP) are not different from those of CCN except for the fact that the concentration of background aerosols acting as CCN is 100 times higher than the concentration of background aerosols acting as INP at each time step and grid point, following a general difference between CCN and INP in terms of their concentrations (Pruppacher and Klett, 1978).

Once clouds form and background aerosols start to be in clouds, those aerosols are not background aerosols anymore and the size distribution and concentrations of those aerosols begin to evolve through aerosol sinks and sources that include advection and aerosol activation (Fan et al., 2009). For example, once aerosols are activated, they are removed from the corresponding bins of the aerosol spectra. In clouds, after aerosol activation, aerosol mass starts to be inside hydrometeors and via collision-collection, it transfers to different types and sizes of hydrometeors. In the end, aerosol mass disappears in the atmosphere when hydrometeors with aerosol mass touches the surface. In non-cloudy areas, aerosol size and spatial distributions are designed to be identical to the size and spatial distributions of background aerosols, respectively. In other words, for this study, we use “the aerosol recovery method”. In this method, at any grid points, immediately after clouds disappear entirely, aerosol size distributions and number concentrations recover to background properties that background aerosols at those points have before those points are included in clouds. In this way, we can keep aerosol concentrations outside clouds in the simulations at observed counterparts. Thus, we are able to simulate aerosol evolutions, via processes such as transportation of background aerosols by wind (or aerosol advection),

https://doi.org/10.5194/acp-2021-917
Preprint. Discussion started: 15 December 2021


Atmospheric Chemistry and Physics Discussions

as observed, in case we neglect possible errors from the assumption on aerosol size distribution and composition, and the process where observed data are interpolated or extrapolated to grid points and time steps in the simulations. In the aerosol recovery method, there is no time interval between the cloud disappearance and the aerosol recovery. Here, when the sum of mass of all types of hydrometeors (i.e., water drops, ice crystals, snow aggregates, graupel and hail) is not zero at a grid point, that grid point is considered to be in clouds. When this sum becomes zero, clouds are considered to disappear. Many studies using CSRM have employed this aerosol recovery method. They have proven that with the recovery method, reasonable simulations of overall cloud and precipitation properties are accomplished (e.g., Morrison and Grabowski, 2011; Lebo and Morrison, 2014; Lee et al., 2016; Lee et al., 2018).

3.3 Additional runs

We repeat the control-s run by getting rid of aerosol-advection induced increases in aerosol concentrations as a way of investigating how the aerosol advection affects the cloud system in the Seoul area. This repeated run is named the low-aerosol-s run. An aerosol layer, which is advected from East Asia or from the west of the Seoul area to it, increases aerosol concentrations in the Seoul area. There are stations in islands in the Yellow Sea that monitor the aerosol advection (Eun et al., 2016; Ha et al., 2019). To monitor and identify the aerosol advection, PM_{10} and $PM_{2.5}$ which are measured by a station in Baekryongdo island in Yellow Sea are compared to those which are measured in stations in and around the Seoul area. In Figure 2a, a dot and a rectangle mark the island and the Seoul area, respectively. The time evolution of $PM_{2.5}$ measured by the station on the island and the average $PM_{2.5}$ over stations in the Seoul area, between 07:00 LST on December 22nd and 21:00 LST on December 24th in 2017 when there is the strong advection of aerosols from East Asia to the Seoul area, is shown in Figure 4. At 09:00 LST on December 22nd, the advection of aerosols from East Asia enables aerosol mass to start going up and attain its peak around 05:00 LST on December 23rd on the island. Following this, aerosol mass starts to increase in the Seoul area around 01:00 LST on December 23rd, and the mass attains its

https://doi.org/10.5194/acp-2021-917
Preprint. Discussion started: 15 December 2021


Atmospheric Chemistry and Physics Discussions

peak at 15:00 LST on December 23rd in the Seoul area. This is because aerosols, which are advected from East Asia, move through the island to reach the Seoul area.

In the low-aerosol-s run, as a way of getting rid of the increase in aerosol concentrations, it is assumed that PM2.5 and thus background aerosol concentrations after 01:00 LST on December 23rd do not evolve with the aerosol advection in the Seoul area. Hence, the background concentration of aerosols acting as CCN is assumed to have that at 01:00 LST on December 23rd at each time step and grid point at the beginning of the simulation period. However, background aerosol concentration acting as INP at each time step and grid point in the low-aerosol-s run is not different from that in the control-s run during the simulation period. In the observed PM data for the Seoul area, there is reduction in PM by a factor of ~10 on average over a period between ~07:00 and ~14:00 LST on December 24th, since precipitation scavenges aerosols (Figure 4). To emulate this scavenging and reflect it in background aerosols for the low-aerosol-s run, PM2.5 and corresponding background aerosol concentrations at each grid point is gradually reduced for the period between 07:00 and 14:00 LST on December 24th. This reduction is done in a way that background aerosol concentration at each grid point at 14:00 LST on December 24th is 10 times lower than that at 07:00 LST on December 24th in the low-aerosol-s run. Then, PM2.5 and corresponding background aerosol concentrations at each grid point at 14:00 LST on December 24th maintains until the end of the simulation period. This results in the evolution of the average PM2.5 over the Seoul area in the low-aerosol-s run as shown in Figure 4. Here, the concentration of background aerosols acting as CCN, which is averaged over the whole domain and simulation period, in the control-s run is 3.1 times higher than that in the low-aerosol-s run. Via comparisons between the runs, how the increasing concentration of background aerosols acting as CCN due to the aerosol advection has an impact on clouds can be examined. The concentration of background aerosols acting as CCN is different among grid points and time steps in the control-s run. Hence, the ratio of the concentration of background aerosols acting as CCN between the runs is different among gird points and time steps.

For the Beijing case, to examine how aerosols affect clouds and precipitation, we repeat the control-b run with simply reduced concentrations of background aerosols acting as CCN at each time step and grid point by a factor of 3.1. This repeated run is named the

https://doi.org/10.5194/acp-2021-917
Preprint. Discussion started: 15 December 2021


Atmospheric Chemistry and Physics Discussions

low-aerosol-b run. The 3.1-fold increase in aerosol concentrations from the low-aerosol-b run to the control-b is based on the 3.1-fold increase in the average concentration of background aerosols acting as CCN from the low-aerosol-s run to the control-s run. However, as in the control-s and low-aerosol-s runs, background aerosol concentration acting as INP at each time step and grid point in the low-aerosol-b run is identical to that in the control-b run during the simulation period. Hence, on average, a pair of the control-s and low-aerosol-s runs has the same aerosol perturbation as in a pair of the control-b and low-aerosol-b runs. Here, we define aerosol perturbation as a relative increase in aerosol concentration when compared to that before the increase occurs. The brief summary of all simulations in this study is given in Table 1.

4. Results

4.1 Cumulative precipitation

The automatic weather system (AWS) operates at the surface and rain gauges in the AWS measure precipitation hourly with a spatial resolution of ~1 km. We compare the observed precipitation to the simulated counterpart in the control-s run for the Seoul case and in the control-b run for the Beijing case. For this comparison, the observed and simulated precipitation rates at the surface are averaged over the domain for each of the Seoul and Beijing cases (Figures 5a and 5b). Here, the simulated precipitation rates are smoothed over 1 hour. The comparison shows that the evolution of the simulated precipitation rate does not deviate from the observed counterpart significantly (Figures 5a and 5b).

In the Seoul case, overall, the precipitation rate is higher in the control-s run than in the low-aerosol-s run. As a result of this, the domain-averaged cumulative precipitation amount at the last time step is 14.1 mm and 12.0 mm in the control-s run and the low-aerosol-s run, respectively. The control-s run shows ~20 % higher cumulative precipitation amount. In the Beijing case, the evolution of the mean precipitation rate in the control-b run is not significantly different from that in the low-aerosol-b run. Due to this, the control-b run shows only ~2% higher cumulative precipitation amount, despite the fact that the concentrations of background aerosols are ~3 times higher in the control-b run than in the

https://doi.org/10.5194/acp-2021-917
Preprint. Discussion started: 15 December 2021


Atmospheric Chemistry and Physics Discussions

low-aerosol-b run. Note that in the Seoul case, the time- and domain-averaged concentration of background aerosols is also ~3 times higher in the control-s run than in the low-aerosol-s run. Despite this, the difference in the cumulative precipitation amount between the runs with different concentrations of background aerosols is greater in the Seoul case than in the Beijing case.

4.2 Precipitation, and associated latent-heat and dynamic processes

Figures 6a and 6b show the cumulative frequency distributions of precipitation rates at the last time step in the simulations for the Seoul and Beijing cases, respectively. In each of those figures, the observed frequency distribution is shown and compared to the simulated distribution. The observed distribution is obtained by interpolating and extrapolating the observed precipitation rates to grid points and time steps in each of the control-s and control-b runs. The observed maximum precipitation rates are 13.0 and 44.5 mm hr^{-1} for the Seoul and Beijing cases, respectively, and these maximum rates are similar to those in the control-s and control-b runs, respectively. Overall, the observed and simulated frequency distributions are in good agreement for each of the cases. This enables us to assume that results in the control-s (control-b) run are benchmark results to which results in the low-aerosol-s (low-aerosol-b) run can be compared to identify how aerosols have an impact on clouds and precipitation for the Seoul (Beijing) case. Here, it is notable that for the Beijing case, while differences in the cumulative precipitation amount between the control-b and low-aerosol-b runs are not significant, features in the frequency distribution of precipitation rates between those runs are substantially different (Figure 6b).

1) Seoul case

a. Precipitation Frequency distributions

Regarding precipitation whose rates are higher than ~2 mm hr^{-1}, the cumulative precipitation frequency at the last time step is higher in the control-s run as compared to that in the low-aerosol-s run (Figure 6a). There are increases in the cumulative frequency

https://doi.org/10.5194/acp-2021-917
Preprint. Discussion started: 15 December 2021


Atmospheric Chemistry and Physics Discussions

by a factor of as much as ~10 in the control-s run when it comes to specific ranges of precipitation whose rates are higher than ~2 mm hr^{-1}. When it comes to precipitation rates above ~11 mm hr^{-1}, precipitation is present in the control-s run and precipitation is absent in the low-aerosol-s run. Regarding precipitation whose rates are lower than ~2 mm hr^{-1}, differences in the cumulative frequency between the runs are insignificant. Hence, we see that there are significant increases in the frequency of relatively heavy precipitation whose rates are above ~2 mm hr^{-1} in the control-s run when compared to that in the low-aerosol-s run. At the last time step, this results in a larger amount of cumulative precipitation in the control-s run than in the low-aerosol-s run.

The time evolution of the cumulative precipitation frequency is shown in Figure 7. At 06:00 LST December 24th 2017, which corresponds to the initial stage of the precipitation development, the maximum precipitation rate reaches ~3 mm hr^{-1} and there is the greater frequency over most of precipitation rates in the control-s run than in the low-aerosol-s run. With the time progress from 06:00 to 10:00 LST, the maximum precipitation rate increases to reach 12 mm hr^{-1} and the cumulative frequency is higher over precipitation whose rates are higher than ~3 mm hr^{-1} in the control-s run, while for precipitation whose rates are lower than ~3 mm hr^{-1}, differences in the cumulative frequency between the runs are negligible (Figures 7a, 7b, 7c and 7d). When time reaches 12:00 LST, which is around a time when the peak in the evolution of the area-averaged precipitation rates occurs and thus the system is at its mature stage, the maximum precipitation rate increases up to ~13 mm hr^{-1}. The basic patterns of differences in the cumulative precipitation frequency between the runs with the maximum precipitation rate around 13 mm hr^{-1}, which are established at 12:00 LST, maintain until the end of the simulation period (Figures 6a and 7e).

b. Condensation, deposition, updrafts and associated variables

Note that the source of precipitation is precipitable hydrometeors which are raindrops, snow, graupel and hail particles. Droplets and ice crystals are the source of those precipitable hydrometeors mostly via collision and coalescence among droplets and ice crystals. Droplets and ice crystals gain their mass via condensation and deposition, respectively. Based on this, to explain the greater cumulative precipitation amount in the

https://doi.org/10.5194/acp-2021-917
Preprint. Discussion started: 15 December 2021


Atmospheric Chemistry and Physics Discussions

control-s run than in the low-aerosol-s run, the evolutions of differences in condensation, deposition and associated updrafts between the runs are analyzed. The vertical profiles of differences in the area-averaged condensation and deposition rates, updraft mass fluxes and associated variables between the runs at 03:20, 03:40, 06:00 and 12:00 LST are shown in Figure 8. Condensation rates in the control-s run start to be larger than that in the low-aerosol-s run throughout all altitudes at 03:20 LST (Figure 8a). Higher aerosol concentrations induce more nucleation of droplets and associated greater integrated surface of droplets. Hence, more droplet surface is provided for water vapor to condense onto. This induces more water vapor to be condensed to lead to more condensation in the control-s run. This establishes stronger feedbacks between updrafts and condensation, leading to greater droplet (or cloud-liquid) mass (Figure 8a). Then, these stronger feedbacks, which involve stronger updrafts particularly above 2 km in altitude, subsequently induce greater deposition and snow mass at 03:40 LST in the control-s run.

Through aerosol-induced stronger feedbacks between condensation, deposition and updrafts in the control-s run, differences in condensation and deposition between the control-s and low-aerosol-s runs increase as time progresses from 03:40 LST to 06:00 LST (Figures 8b and 8c). At 06:00 LST, there is more freezing starting to occur in the control-s run than in the low-aerosol-s run. However, differences in freezing are two to three orders of magnitude smaller than those in condensation and deposition. A similar situation in terms of relative differences between freezing, condensation and deposition continues after 06:00 LST until time reaches 12:00 LST when the overall differences in the cumulative precipitation frequency between the runs are established (Figures 8c and 8d). It is notable that at 12:00 LST, the freezing rate becomes lower in the control-s run. Hence, here, we see that aerosol-induced more cumulative precipitation amount and associated differences in the precipitation frequency distribution between the control-s and low-aerosol-s runs are primarily associated with aerosol-induced more condensation which induce aerosol-induced more deposition but weakly connected to aerosol-induced changes in freezing.

c. Condensation frequency distributions and horizontal distributions of condensation and precipitation

https://doi.org/10.5194/acp-2021-917
Preprint. Discussion started: 15 December 2021


Atmospheric Chemistry and Physics Discussions

Based on the importance of condensation for aerosol-induced changes in precipitation, the horizontal distribution of the column-averaged condensation rates over the domain and the cumulative frequency distribution of the column-averaged condensation rates at each time step is obtained. To better visualize the role of condensation in precipitation, the horizontal distribution of the column-averaged condensation rates is superimposed on that of precipitation rates (Figure 9). At 03:40 LST, condensation mainly occurs around the northern part of the domain as marked by a yellow rectangle. The synoptic wind condition in the marked area favors the collision between northward and southward wind and the associated convergence around the surface (Figures 9a and 9b). This convergence induces updrafts and condensation in the marked area. In the marked area, more aerosols induce more and more extensive condensation, which leads to the higher domain-averaged condensation rates in the control-s run than in the low-aerosol-s run (Figures 8b, 9a and 9b). More droplets are formed on more aerosols and more droplets provide more surface areas where condensation occurs and this enables more and more extensive condensation in the control-s run than in the low-aerosol-s run (Figures 8b, 9a and 9b). At 06:20 LST, a precipitating system is advected into the domain via the western boundary (Figures 9c and 9d). As seen in Figures 9c, 9d, 9e and 9f for 06:20 and 07:20 LST, respectively, as time progresses from 06:20 to 07:20 LST, the advected precipitating system is further advected to the east and extended mostly over areas in the northern part of the domain where condensation mainly occurs. This confirms that condensation is the main source of cloud mass and precipitation. In the eastern part of the domain, there are mountains and in particular, higher mountains are on the northeastern part of the domain than in the other parts of the domain. These higher mountains induce forced convection and associated condensation more effectively in the northeastern part than in the other parts. This is in favor of the precipitating system that extends further to the east in the northern part of the domain. Due to more aerosols, condensation, which is induced by forced convection over mountains, is more and more extensive in the control-s run (Figures 9c, 9d, 9e and 9f).

As time progresses to 08:40 LST, the precipitating system moves eastward further in the northern part of the domain and the system in the control-s run extends to the east further as compared to that in the low-aerosol-s run (Figures 9g, 9h, 9i, 9j, 9k and 9l). In association with more aerosols and associated more condensation over mountains in the

https://doi.org/10.5194/acp-2021-917
Preprint. Discussion started: 15 December 2021


Atmospheric Chemistry and Physics Discussions

northeastern part, there is more extension of the system in the control-s run than in the low-aerosol-s run. This enables the system in the control-s run to reach the eastern boundary at 08:40 LST, which is earlier than in the low-aerosol-s run. The system in the low-aerosol-s run reaches the eastern boundary at 09:00 LST (Figure 9n). Here, we see that although aerosols do not change overall locations of the precipitation system, they affect how fast the system extends to the east by affecting the amount of condensation which is produced by forced convection. Associated with this, as seen in Figure 10, the control-s run has the much higher cumulative condensation frequency than the low-aerosol-s run over all of condensation rates during the period between 07:20 and 09:00 LST. Contributed by this, the higher precipitation frequency over most of precipitation rates occurs in the control-s run during the period (Figures 7b and 7c).

At 10:00 LST, in the southern part of the domain, there is a precipitating area forming as marked by a yellow rectangle (Figures 9o and 9p). The precipitation area in the southern part of the domain extends and merge into the advecting main precipitating system in the northern part of the domain during the period between 10:20 and 11:00 LST (Figures 9q, 9r, 9s and 9t). The merge leads to precipitation that occupies most of the domain at 12:00 LST (Figures 9u and 9v). After 10:00 LST, associated with this merge, the maximum precipitation rate increases to 13 mm hr^{-1} at 12:00 LST (Figures 7e). After 13:00 LST, the precipitation enters its dissipating stage and its area reduces and nearly disappears during the period between 13:00 and 15:20 LST (Figures 9w, 9x, 9y and 9z). Even after the merge, aerosol-induced more condensation maintains and this in turn contributes to a situation where the control-s run has the greater precipitation frequency over most of precipitation rates than in the low-aerosol-s run until the simulations progress to their last time step (Figures 6a, 7e and 8d).

2) Beijing case

Stronger convection and deeper clouds develop in the Beijing case than in the Seoul case. The maximum cloud depth is ~ 7 and 12 km in the control-s and control-b runs, respectively. In the Seoul case, clouds do not reach the tropopause, while they reach the tropopause in the Beijing case. Deeper clouds in the Beijing case produce the maximum precipitation rate

https://doi.org/10.5194/acp-2021-917
Preprint. Discussion started: 15 December 2021


Atmospheric Chemistry and Physics Discussions

of ~45 mm hr^{-1} in the control-b run. However, less deep clouds in the Seoul case produce the maximum precipitation rate of ~13 mm hr^{-1} in the control-s run (Figure 6).

a. Precipitation frequency distributions

When it comes to precipitation whose rates are higher than ~12 mm hr^{-1}, the control-b run has the higher cumulative precipitation frequency at the last time step than the low-aerosol-b run (Figure 6b). The cumulative frequency increases by a factor of as much as ~10 with respect to some ranges of precipitation rates above ~12 mm hr^{-1}. Moreover, regarding precipitation rates higher than ~33 mm hr^{-1}, precipitation is present in the control-b run, however, precipitation is absent in the low-aerosol-b run. Hence, we see that the frequency of comparatively heavy precipitation whose rates are higher than ~12 mm hr^{-1} rises significantly in the control-b run as compared to that in the low-aerosol-b run. Below ~2 mm hr^{-1}, there is also the greater precipitation frequency in the control-b run than in the low-aerosol-b run. Unlike the situation for precipitation rates above ~12 mm hr^{-1} and below ~2 mm hr^{-1}, for precipitation rates from ~2 to ~12 mm hr^{-1}, the control-aerosol-b run has the lower precipitation frequency than in the low-aerosol-b run. Here, we see that the higher precipitation frequency above ~12 mm hr^{-1} and below ~2 mm hr^{-1} balances out the lower precipitation frequency between ~2 and ~12 mm hr^{-1} in the control-b run. This results in the similar cumulative precipitation amount between the runs.

Figure 11 shows the time evolution of the cumulative precipitation frequency. When precipitation starts around 16:00 LST, the higher precipitation frequency occurs over most of precipitation rates in the low-aerosol-run-b run than in the control-b run (Figure 11a). At 16:00 LST, the maximum precipitation rate is lower than 1.0 mm hr^{-1} for both of the runs. As the time progresses to 17:00 LST, the maximum precipitation rate increases to ~17 mm hr^{-1}, and the cumulative precipitation frequency starts to be higher (lower) over precipitation rates higher than ~12 mm hr^{-1} (between ~2 and ~12 mm hr^{-1}) in the control-b run than in the low-aerosol-b run (Figure 11b). At 17:20 LST, the frequency starts to be greater when it comes to precipitation rates below 2 mm hr^{-1} together with those above ~ 12 mm hr^{-1} in the control-b run, while the lower frequency between 2 and 12 mm hr^{-1} in the control-b run maintains (Figure 11c). At 17:20 LST, the maximum precipitation rate

https://doi.org/10.5194/acp-2021-917
Preprint. Discussion started: 15 December 2021


Atmospheric Chemistry and Physics Discussions

increases to 42 (19) mm hr^{-1} in the control-b (low-aerosol-b) run (Figure 11c). At 19:00 LST, the maximum precipitation rate increases to ~45 (33) mm hr^{-1} for the control-b (low-aerosol-b) run, while the qualitative nature of differences in the precipitation frequency distributions with the tipping precipitation rates of ~2 and ~12 mm hr^{-1} between the runs does not vary much between 17:20 and 19:00 LST (Figures 11c and 11d). The qualitative nature of differences in the cumulative precipitation frequency between the runs and the maximum precipitation rates in each of the runs, which are established at 19:00 LST, do not vary significantly until the end of the simulation period (Figures 6b and 11d).

b. Condensation, deposition, updrafts and associated variables

As done for the Seoul case, as a way of better understanding differences in the cumulative precipitation amount and frequency between the control-b and low-aerosol-b runs, the evolutions of differences in the vertical distributions of the area-averaged condensation rates, deposition rates, freezing rates, cloud-liquid and snow mass density and updrafts mass fluxes are obtained and shown in Figures 12. As seen in Figure 5b, precipitation starts around 16:00 LST but differences in condensation rates start at 14:20 LST with higher condensation rates in the control-b run (Figure 12a). Similar to the situation in the Seoul case, higher aerosol concentrations induce more nucleation of droplets and associated greater integrated surface of droplets. Hence, more droplet surface is provided for water vapor to condense onto. This induces more water vapor to be condensed to leads to more condensation in the control-b run. Due to this, cloud liquid as a source of precipitation becomes greater in the control-b run (Figure 12a). Increased condensation rates induce increased condensational heating and thus intensified updrafts (Figure 12a). When time reaches 15:40 LST, deposition rates start to show differences between the runs, however, unlike the situation in the Seoul case, higher aerosol concentrations results in lower deposition rates in the control-b run (Figure 12b). When time reaches 16:00 LST, differences in freezing start to occur and freezing rates are lower in the control-b run (Figure 12c). However, due to stronger updrafts, which are mainly ascribed to more condensation, deposition rates start to be higher in the control-b run at a portion of altitudes with non-zero differences in deposition rates between the runs (Figure 12c). At 17:20 LST,

https://doi.org/10.5194/acp-2021-917
Preprint. Discussion started: 15 December 2021


Atmospheric Chemistry and Physics Discussions

552 due to stronger updrafts again, which are in turn mainly due to more condensation, freezing
553 rates also start to be higher in the control-b run at a portion of altitudes with non-zero
554 differences in freezing rates between the runs (Figure 12d). As the time progresses to 19:00
555 LST, deposition rates are lower in the control-b run over most of the altitudes with non-
556 zero differences in deposition rates between the runs and freezing rates are lower in the
557 control-b run over all of altitudes with non-zero differences in freezing rates between the
558 runs (Figure 12e). As the time progresses to 19:00 LST, higher condensation rates maintain
559 in the control-b run over most of the altitudes with non-zero differences in condensation
560 rates between the runs (Figure 12e). Here, differences in freezing rates are two to three
561 orders of magnitude smaller than those in condensation and deposition between the runs.
562 Associated with this, the time- and domain-averaged deposition and freezing (condensation)
563 rates are lower (higher) in the control-b run over the whole simulation period, although the
564 average differences in freezing rates are negligible as compared to those in deposition rates
565 between the runs. Hence, more condensation (but not deposition and freezing) is a main
566 cause of stronger updrafts in the control-b run. Remember that condensation (deposition
567 and freezing) acts as a source of droplets (ice crystals) which are in turn a source of
568 precipitable hydrometeors and precipitation through collision and coalescence processes.
569 Thus, more condensation tends to induce increases in the precipitation rate in the control-
570 b run. Less deposition and freezing tend to induce decreases in precipitation rate in the
571 control-b run. This competition between condensation, deposition and freezing leads to
572 negligible differences in the cumulative precipitation amount at the last time step between
573 the control-b and low-aerosol-b runs, although roles of freezing in this competition are
574 negligible as compared to those of condensation and deposition.
575
576 **c. Condensation frequency distributions, horizontal distributions of**
577 **condensation and precipitation, and condensation-precipitation**
578 **correlations**
579
580 Figure 13 shows the horizontal distribution of the column-averaged condensation rates over
581 the domain and Figure 14 shows the cumulative frequency distributions of column-
582 averaged condensation rates at selected times. As in the Seoul case, the horizontal

https://doi.org/10.5194/acp-2021-917
Preprint. Discussion started: 15 December 2021


Atmospheric Chemistry and Physics Discussions

583 distribution of condensation rates is superimposed on that of precipitation rates and the
584 terrain in Figure 13. At 14:20 LST, condensation starts to occur in places with mountains,
585 which induce forced convection, and condensation is concentrated around the center of the
586 domain as marked by a yellow circle (Figures 13a and 13b). Note that condensation does
587 not occur in the plain area which is the south of the 100-m terrain-height contour line
588 (Figures 13a and 13b). Due to higher aerosol concentrations, there is more condensation
589 around the center in the control-b run than in the low-aerosol-b run (Figures 13a and 13b).
590 This leads to a situation where the control-b run has the higher area-averaged condensation
591 rates than the low-aerosol-b run (Figure 12a). Then, as time progresses to 17:20 LST, the
592 condensation area extends to the eastern and western parts of the domain mostly over
593 mountain areas (Figures 13c and 13d). Hence, the main source of condensation is
594 considered to be forced convection over mountains. As seen in Figures 13c and 13d, higher
595 aerosol concentrations induce the control-b run to have much more condensation spots and
596 thus much bigger areas with condensation than the low-aerosol-b run at 17:20 LST.
597 Associated with this, aerosol-induced more condensation in the control-b run maintains
598 with the time progress to 17:20 LST (Figure 12d). At 17:20 LST, precipitation mainly
599 occurs in a spot which is in the western part of areas with relatively high condensation rates
600 (Figures 13c and 13d).
601 At 17:20 LST, as seen in the cumulative frequency of condensation rates, the control-
602 b run has the higher condensation frequency above condensation rate of ~10 $\times 10^{-6}$ g m^{-3} s^{-1}
603 and below that of ~3$\times 10^{-6}$ g m^{-3} s^{-1} than the low-aerosol-b run (Figure 14a). This pattern
604 of differences in the condensation frequency distribution with the tipping condensation-
605 rate points at ~10 $\times 10^{-6}$ and ~3 $\times 10^{-6}$ g m^{-2} s^{-1} continues up to 19:00 LST (Figures 14b).
606 Figure 15 shows the mean precipitation rate over each of the column-averaged
607 condensation rates for the period up to 17:20 LST in the control-b run. A column-averaged
608 condensation rate in an air column with a precipitation rate at its surface is obtained and
609 these condensation and precipitation rates are paired at each column and time step. Then,
610 collected precipitation rates are classified and grouped based on the corresponding paired
611 column-averaged condensation rates. The classified precipitation rates corresponding to
612 each of the column-averaged condensation rates are averaged arithmetically to construct
613 Figure 15. There are only less than 10% differences in the mean precipitation rate for each

https://doi.org/10.5194/acp-2021-917
Preprint. Discussion started: 15 December 2021


Atmospheric Chemistry and Physics Discussions

of the column-averaged condensation rates between the control-b and low-aerosol-b runs (not shown). Figure 15 shows that generally a higher condensation rate is related to a higher mean precipitation rate. It is also roughly shown that, according to the mean precipitation rate for each condensation rate, overall, condensation rates below ~3×10^{-6} g m^{-3} s^{-1} and above ~10×10^{-6} g m^{-3} s^{-1} are correlated with precipitation rates below ~2 mm hr^{-1} and above ~12 mm hr^{-1}, respectively, while condensation rates between ~3 and ~10×10^{-6} g m^{-3} s^{-1} are correlated with precipitation rates between ~2 and ~12 mm hr^{-1} (Figure 15). Hence, on average, the higher frequency of condensation with rates above ~10×10^{-6} g m^{-3} s^{-1} and below ~ 3×10^{-6} g m^{-3} s^{-1} can be considered to lead to the higher frequency of precipitation whose rates are higher than ~ 12 mm hr^{-1} and lower than ~ 2 mm hr^{-1} in the control-b run, respectively. It can also be considered that the lower condensation frequency between ~3 and ~10×10^{-6} g m^{-3} s^{-1} leads to the lower precipitation frequency between ~2 and ~12 mm hr^{-1} in the control-b run. At 17:20 LST, the larger precipitation frequency between ~2 and ~12 mm hr^{-1} in the low-aerosol-b run nearly offsets the larger precipitation frequency in the other ranges of precipitation rates in the control-b run (Figure 11c). This leads to the similar average precipitation rate between the runs at 17:20 LST and contributes to the similar cumulative precipitation at the last time step between the runs (Figure 5b).

d. Evaporation and gust fronts

As time progresses from 17:00 to 19:00 LST, the precipitation system moves northward (Figure 16). At the core of the precipitation system, due to evaporation and downdrafts, there is the horizontal outflow forming at 17:00 LST (Figures 16a and 16b). The core is represented by the field of precipitation whose rates are higher than 1 mm hr^{-1} in Figure 16. At the core, the northward outflow is magnified by the northward synoptic-scale wind, while at the core, the outflow in the other directions is offset by the northward synoptic-scale wind. Hence, the outflow is mainly northward from 17:00 LST onwards as marked by yellow circles in Figures 16. This enables convergence or a gust front, which is produced by the outflow from the core, to be mainly formed at the north of the core. Note that the intensity of a gust front is proportional to that of outflow from a core of precipitation or

https://doi.org/10.5194/acp-2021-917
Preprint. Discussion started: 15 December 2021


Atmospheric Chemistry and Physics Discussions

convective system (Weisman and Klemp, 1982; Houze, 1993). The strong gust front at the north of the core generates strong updrafts, a significant amount of condensation and precipitation. Then, a subsequent area with clouds and precipitation is formed at the north of the core as time progresses, which means that the precipitation system extends or moves to the north as seen in comparisons between sub-panels with different times in Figure 16. This movement, which is induced by collaborative work between outflow, synoptic wind and gust fronts, is typical in deep convective clouds.

During the period between 17:00 and 19:00 LST, the time- and domain-averaged cloud-liquid or droplet evaporation rate is higher and downdrafts are stronger, although the control-b run has the lower average rain evaporation rate than the low-aerosol-b run (Figure 17). This is consistent with the numerous previous studies that have shown more evaporation of droplets and associated stronger downdrafts with higher aerosol concentrations (e.g., Tao et al., 2007; Tao et al., 2012; Khain et al., 2008; Lee et al., 2018). Due to higher condensation rates and lower autoconversion rates, the control-b run has more cloud liquid or droplets as a source of evaporation and this enables more evaporative cooling and stronger downdrafts in the control-b run. For the period from 17:00 to 19:00 LST, with the development of convergence or the gust front, as mentioned above, the maximum precipitation rate increases from ~ 17 (17) to ~ 45 (33) mm hr^{-1} in the control-b (low-aerosol-b) run (Figure 11). This indicates that the gust-front development contributes to the overall intensification of the precipitation system, while it moves northward. If there were only northward synoptic-scale wind with no formation of the gust front, the system would move northward with less intensification. Over the period from 17:00 to 19:00 LST, stronger downdrafts and associated stronger outflow generate a stronger gust front and more subsequent condensation, leading to a situation where the control-b run has the higher maximum precipitation rate than the low-aerosol-b run. Around 19:00 LST, the system enters its dissipating stage, accompanying reduction in the precipitating area and the area-averaged precipitation rate (Figures 5b, 16m and 16n).

e. Moist static energy

https://doi.org/10.5194/acp-2021-917
Preprint. Discussion started: 15 December 2021


Atmospheric Chemistry and Physics Discussions

675 Analyses to construct Figure 15 are repeated only for a time point at 16:30 LST and they
676 indicate that as shown in Figure 15 for the period up to 17:20 LST, the column-averaged
677 condensation rates above 10 $\times 10^{-6}$ g m^{-3} s^{-1} and below 3×10^{-6} g m^{-3} s^{-1} correspond to
678 precipitation rates above 12 mm hr^{-1} and below 2 mm hr^{-1}, respectively, at 16:30 LST.
679 According to those analyses, condensation rates between 3×10^{-6} g m^{-3} s^{-1} and 10 $\times 10^{-6}$ g
680 m^{-3} s^{-1} correspond to precipitation rates between 2 and 12 mm hr^{-1} at 16:30 LST.
681 Condensation, which controls droplet mass and precipitation, is controlled by updrafts and
682 updrafts are in turn controlled by instability. One of important factors that maintain
683 instability is the moist static energy. Motivated by this, to better understand differences in
684 the precipitation frequency distribution in association with those in the condensation
685 frequency distribution between the control-b and low-aerosol-b runs, we calculate the flux
686 of the moist static energy and the flux is defined as follows:
687
688 $$\overrightarrow{Fs} = S \times \rho \times \vec{V} \qquad (1),$$
689
690 where $\overrightarrow{Fs}$ represents the flux of the moist static energy, S the moist static energy, ρ the air
691 density and $\vec{V}$ the horizontal-wind vector. In Eq. (1), we see that the flux is in the vector
692 form and has two components, which are its magnitude and direction. The fluxes of the
693 moist static energy in the PBL are obtained over the domain at 16:30 LST, since in general,
694 the moist static energy in the PBL has much stronger effects on instability and updrafts
695 than that above the PBL. In particular, as diagrammatically depicted in Figure 18, we focus
696 on the PBL fluxes of the energy that cross the boundary over a time step at 16:30 LST
697 between areas with the column-averaged condensation rate from 3×10^{-6} g m^{-3} s^{-1} to 10
698 $\times 10^{-6}$ g m^{-3} s^{-1}, which are referred to as “area A”, and those with the column-averaged
699 condensation rate above 10×10^{-6} g m^{-3} s^{-1}, which are referred to as “area B”. This is because
700 we are interested in the exchange of the moist static energy between areas A and B and this
701 exchange can be seen by looking at those fluxes which cross the boundary between those
702 areas.
703 We are interested in the exchange of the energy, since we hypothesized that the
704 exchange somehow alters instability in each of areas A and B in a way that there are
705 increases (decreases) in instability, the updraft intensity, condensation and precipitation

https://doi.org/10.5194/acp-2021-917
Preprint. Discussion started: 15 December 2021


Atmospheric Chemistry and Physics Discussions

706 with increasing aerosol concentrations in area B (A), leading to the higher (lower)
707 frequency of condensation whose rates are higher than 10×10^{-6} g m^{-3} s^{-1} (between 3×10^{-6}
708 g m^{-3} s^{-1} and 10×10^{-6} g m^{-3} s^{-1}) and precipitation whose rates are higher than 12 mm hr^{-1}
709 (between 2 and 12 mm hr^{-1}) in the control-b run than in the low-aerosol-b run. When the
710 PBL fluxes, which crosses the boundary over the time step at 16:30 LST, are averaged over
711 the domain at 16:30 LST, there is the net flux from area A to area B. This means that there
712 is the net transportation of the moist static energy from areas with condensation rates
713 between 3×10^{-6} g m^{-3} s^{-1} and 10×10^{-6} g m^{-3} s^{-1} to those with condensation rates greater
714 than 10×10^{-6} g m^{-3} s^{-1} in the PBL at 16:30 LST as shown in Table 2. Table 2 shows the
715 average flux of the moist static energy which crosses the boundary between areas A and B
716 in the control-b run as well as the low-aerosol-b run. To calculate the average flux at 16:30
717 LST in Table 2, the fluxes, which cross the boundary between areas A and B over the time
718 step at 16:30 LST, only at grid points in the PBL are summed and divided by the number
719 of all grid points over the whole domain at 16:30 LST. Here, all grid points include grid
720 points with those fluxes crossing the boundary and those without those fluxes including
721 grid points with zero fluxes, and include grid points both in and above the PBL. For the
722 calculation, the flux from area A to area B has a positive sign, while the flux from area B
723 to area A has a negative sign as depicted in Figure 18. Since the average flux is positive
724 for both of the runs, there is on average, the net flux from area A to area B in the PBL. The
725 above-described analysis for the average of the fluxes crossing the boundary between areas
726 A and B is repeated for every time step between 16:30 and 17:00 LST and based on this,
727 the average flux over the period between 16:30 and 17:00 LST is obtained. Analyses to
728 construct Figure 15 are repeated again for a time period between 16:30 and 17:00 LST.
729 These repeated analyses find that as in the situation only for 16:30 LST, the column-
730 averaged condensation rates below 3×10^{-6} g m^{-3} s^{-1} and above 10×10^{-6} g m^{-3} s^{-1}
731 correspond to precipitation rates below 2 mm hr^{-1} and above 12 mm hr^{-1}, respectively,
732 while the column-averaged condensation rates between 3×10^{-6} g m^{-3} s^{-1} and 10×10^{-6} g m^{-3} s^{-1} correspond to precipitation rates between 2 and 12 mm hr^{-1} for every time step between
734 16:30 and 17:00 LST. As shown in Table 2, the average flux for the period between 16:30
735 and 17:00 LST is also positive as in the situation only for 16:30 LST. This means on

https://doi.org/10.5194/acp-2021-917
Preprint. Discussion started: 15 December 2021


Atmospheric Chemistry and Physics Discussions

736 average, there is the net transportation of the moist static energy from area A to area B in
737 the PBL during the period between 16:30 and 17:00 LST.
738 At 16:30 LST, condensation with rates above 10 $\times 10^{-6}$ g m^{-3} s^{-1} starts to develop and
739 this forms area B. Area B has stronger updrafts via greater condensational heating than in
740 other areas, including area A, with lower condensation rates. Stronger updrafts in area B
741 induce the convergence of air and associated moist static energy from area A to area B.
742 Since the average condensation rate and updrafts at 16:30 LST over area B are higher and
743 stronger due to increasing aerosol concentrations, respectively, the air convergence and the
744 associated transportation of the moist static energy in the PBL from area A to area B are
745 stronger and more, respectively, in the control-b run than in the low-aerosol-b run (Table
746 2). Stated differently, area B steals the moist static energy from area A, and this occurs
747 more effectively in the control-b run. This increases instability and further intensifies
748 updrafts in area B, and decreases instability and weakens updrafts in area A, while these
749 increases and decreases (intensification and weakening) of instability (updrafts) are greater
750 in the control-b run for the period from 16:30 to 17:00 LST. This increases condensation,
751 cloud mass and precipitation whose rates are higher than 12 mm hr^{-1} in area B, and
752 decreases condensation, cloud mass and precipitation whose rates are from 2 to 12 mm hr^{-1}
753 in area A. These increases and decreases occur more effectively for the control-b run than
754 for the low-aerosol-b run during the period. This in turn leads to the lower precipitation
755 frequency for the precipitation rates from 2 to 12 mm hr^{-1} and the higher frequency for the
756 precipitation whose rates are higher than 12 mm hr^{-1} at 17:00 LST in the control-b run
757 (Figure 11b). The weakened updrafts and reduced condensation turn a portion of
758 precipitation with rates between 2 and 12 mm hr^{-1} to precipitation whose rates are below 2
759 mm hr^{-1}, and this takes place more efficiently in the control-b run during the period between
760 16:30 and 17:00 LST. This eventually increases the frequency of precipitation rates below
761 2 mm hr^{-1} and this increase is greater for the control-b run, leading to the greater
762 precipitation frequency for the precipitation rates below 2 mm hr^{-1} in the control-b run at
763 17:20 LST (Figure 11c).
764

765 **5. Discussion**

766

https://doi.org/10.5194/acp-2021-917
Preprint. Discussion started: 15 December 2021


Atmospheric Chemistry and Physics Discussions

5.1 Comparison of the Seoul and Beijing cases

In this section, we compare the Seoul case to the Beijing case. To examine aerosol effects on the Beijing case, the control-b and the low-aerosol-b runs are compared, and remember that the low-aerosol-b run is the repeated control-b run by simply reducing the background-aerosol concentrations at each of grid points and time steps by a factor of 3.1. Remember that the low-aerosol-s run is the repeated control-s run and the low-aerosol-s run has the 3.1 times lower concentration of background aerosols, which is averaged over the whole domain and simulation period, than the control-s run. Hence, the relative variation of the average concentration of background aerosols from the control-b run to the low-aerosol-b run is not different from that from the control-s run to the low-aerosol-s run. This enables the two pairs of runs to be compared for an identical magnitude of an aerosol perturbation.

Note that clouds in the Seoul case are less deep as compared to those in the Beijing case. Thus, overall, clouds and associated updrafts in the Seoul case are not as strong as those in the Beijing case. Hence, unlike the situation in the Beijing case, stronger updrafts, which accompany higher condensation rates, and associated convergence in the Seoul case are not strong enough to steal the sufficient amount of the moist static energy from weaker updrafts which accompany lower condensation rates. This makes the redistribution of the moist static energy between areas with relatively higher condensation rates and those with relative lower condensation rates, such as that between areas A and B for the Beijing case, ineffective for the Seoul case. Due to this, the sign of aerosol-induced changes in the frequency of precipitation rates does not vary throughout all of the precipitation rates except for the range of low precipitation rates where there are nearly no aerosol-induced changes in the frequency in the Seoul case as shown in Figure 6a. As seen in Figure 6a, mainly due to increases in condensation and deposition, precipitation frequency increases for most of precipitation rates, although the precipitation frequency does not show significant changes as aerosol concentration increases for relatively low precipitation rates in the control-s run as compared to that in the low-aerosol-s run. This means that there are no tipping precipitation rates where the sign of aerosol-induced changes in the frequency of precipitation rates changes in the Seoul case, contributing to the higher cumulative

https://doi.org/10.5194/acp-2021-917
Preprint. Discussion started: 15 December 2021


Atmospheric Chemistry and Physics Discussions

797 precipitation amount in the simulation with higher aerosol concentrations for the Seoul
798 case, which are different from the situation in the Beijing case.
799 In the Beijing case with deeper clouds as compared to those in the Seoul case, clouds
800 develop gust fronts via strong downdrafts and associated strong outflow. These gust fronts
801 play an important role in developing strong convection and associated high precipitation
802 rates. Unlike the situation in the Seoul case, there are strong clouds and associated updraft
803 entities that are able to steal heat and moisture (or the moist static energy) as sources of
804 instability from areas with relatively less strong clouds and updrafts with medium strength.
805 This further intensifies strong clouds and weakens clouds with medium strength. Due to
806 this, the cumulative frequency of heavy (medium) precipitation in association with strong
807 clouds (clouds with medium strength) increases (decreases). Some of the weakened clouds
808 eventually produce light precipitation, which increase the cumulative frequency for light
809 precipitation. The intensification of strong clouds and the weakening of clouds with
810 medium strength gets more effective with increasing aerosol concentrations. Hence, in the
811 Beijing case, for medium precipitation in association with clouds with medium strength,
812 the simulation with higher aerosol concentrations shows the lower cumulative precipitation
813 frequency at the last time step. However, for heavy precipitation, which is associated with
814 strong clouds, and light precipitation, the simulation with higher aerosol concentrations
815 shows the higher cumulative precipitation frequency at the last time step. These differential
816 responses of precipitation to increasing aerosol concentrations among different types of
817 precipitation occur in the circumstances of the similar cumulative precipitation amount
818 between the simulations with different aerosol concentrations. This similar precipitation
819 amount is due to above-mentioned competition between aerosol-induced changes in
820 condensation, deposition and freezing.
821 In both of the Seoul and Beijing cases, aerosol-induced changes in condensation plays
822 an important role in making differences in the precipitation amount and/or the precipitation
823 frequency distribution between the simulations with different aerosol concentrations. It is
824 notable that in less deep clouds in the Seoul case, in addition to condensation, deposition
825 plays a role in precipitation to induce aerosol-induced increases in the precipitation amount.
826 Aerosol-induced increases in condensation initiate the differences in cloud mass and
827 precipitation and then aerosol-induced increases in deposition follow to further enhance

https://doi.org/10.5194/acp-2021-917
Preprint. Discussion started: 15 December 2021


Atmospheric Chemistry and Physics Discussions

those differences. However, in deep clouds in the Beijing case, condensation tends to induce increases in cloud mass and precipitation with increasing aerosol concentrations, while deposition tend to induce decreases in cloud mass and precipitation with increasing aerosol concentrations. Hence, as clouds get shallower and thus ice processes become less active, the role of ice processes in aerosol-induced changes in precipitation amount turns from aerosol-induced suppression of precipitation to enhancement of precipitation. Here, we find that contrary to the traditional understanding, the role of aerosol-induced variation of freezing in precipitation is not significant as compared to that of condensation and deposition in both of the cases.

6. Summary and conclusions

This study examines impacts of aerosols on clouds and precipitation in two metropolitan areas, which are the Seoul and Beijing areas, in East Asia that has experienced substantial increases in aerosol concentrations over the last decades. The examination is performed via simulations, which use a CSRM. These simulations are for deep clouds which reach the tropopause in the Beijing case and for comparatively less deep clouds which do not reach the tropopause yet grow above the level of freezing in the Seoul case.

In both of the cases, aerosol-induced changes in condensation plays a critical role in aerosol-induced variation of precipitation properties (e.g., the precipitation amount and the precipitation frequency distribution). In the Seoul case, aerosol-induced increases in condensation and subsequent increases in deposition lead to aerosol-induced increases in the precipitation frequency over most of precipitation rates and thus in the precipitation amount; note that condensation and deposition are sources of cloud mass and precipitation. However, in the Beijing case, while there are increases in condensation with increasing aerosol concentrations, there are decreases in deposition with increasing aerosol concentrations. So, there is competition between increases in condensation and decreases in deposition. This competition leads to negligible aerosol-induced changes in cumulative precipitation amount in the Beijing case. Also, there is another competition for the moist static energy among clouds with different updrafts and condensation in the Beijing case.

https://doi.org/10.5194/acp-2021-917
Preprint. Discussion started: 15 December 2021


Atmospheric Chemistry and Physics Discussions

This competition results in aerosol-induced differential changes in the precipitation frequency distributions.

With clouds getting deeper from the Seoul case to the Beijing case, clouds and associated updrafts, which are strong enough to steal the moist static energy from other clouds and their updrafts, appear. This makes strong clouds stronger and clouds with medium strength weaker. With higher aerosol concentrations, strong clouds steal the more energy, and thus strong clouds become stronger and clouds with medium strength weaker with a greater magnitude. As a result of this, there are more frequent heavy precipitation (whose rates are higher than 12 mm hr^{-1}) and light precipitation (whose rates are lower than 2 mm hr^{-1}), and less frequent medium precipitation (with rates from 2 to 12 mm hr^{-1}) with increasing aerosol concentrations in the Beijing case.

In both of the Seoul and Beijing cases, there are mountains and they play an important role in how cloud and precipitation evolve with time and space. In both of the cases, the precipitating system moves or expands over mountains which induce forced convection and generate condensation. This important role of mountains and forced convection in the formation and evolution of the precipitation system has not been examined much in the previous studies of aerosol-cloud interactions, since many of those previous studies (e.g., Jiang et al., 2006; Khain et al., 2008; Li et al., 2011; Morrison et al., 2011) have dealt with convective clouds that develop over plains and oceans. Hence, findings in this study, which are related to mountain-forced convection and its interactions with aerosols, can be complementary to those previous studies. Stated differently, this study can shed light on our path to the understanding of aerosol-cloud interactions over more general domains not only with no terrain but also with terrain.

https://doi.org/10.5194/acp-2021-917
Preprint. Discussion started: 15 December 2021

Atmospheric Chemistry and Physics Discussions

889 **Code/Data availability**

890

891 Our private computer system stores the code/data which are private and used in this study.
892 Upon approval from funding sources, the data will be opened to the public. Projects related
893 to this paper have not been finished, thus, the sources prevent the data from being open to
894 the public currently. However, if information on the data is needed, contact the
895 corresponding author Seoung Soo Lee (slee1247@umd.edu).

896

897 **Author contributions**

898 Essential initiative ideas are provided by SSL, KJH and KHS to start this work. Simulation
899 and observation data are analyzed by SSL, JC and GK. JU and YZ reviewed the results and
900 contributed to their improvement.

901

902 **Competing interests**

903 The authors declare that they have no conflict of interest.

904

905 **Acknowledgements**

906 This study is supported by the National Research Foundation of Korea (NRF) grant funded
907 by the Korea government (MSIT) (No. NRF2020R1A2C1003215), the “Construction of
908 Ocean Research Stations and their Application Studies” project funded by the Ministry of
909 Oceans and Fisheries, South Korea. Authors thank Danhong Dong at Chinese Academy of
910 Sciences and Fang Wu at Beijing Normal University for their reviewing this paper.

911

912

913

914

915

916

917

918

919

920

https://doi.org/10.5194/acp-2021-917
Preprint. Discussion started: 15 December 2021

Atmospheric Chemistry and Physics Discussions

References

Chen, F., and Dudhia, J.: Coupling an advanced land-surface hydrology model with the Penn State-NCAR MM5 modeling system. Part I: Model description and implementation, Mon. Wea. Rev., 129, 569–585, 2001.

Dong, B., Wilcox, L. J., Highwood, E. J., and Sutton, R. T.: Impacts of recent decadal changes in Asian aerosols on the East Asian summer monsoon: roles of aerosol–radiation and aerosol–cloud interactions, Clim. Dyn., 53, 3235-3256, 2019.

Eun, S.-H., Kim, B.-G., Lee, K.-M., and Park, J.-S.: Characteristics of recent severe haze events in Korea and possible inadvertent weather modification, SOLA, 12, 32-36, 2016.

Fan, J., Yuan, T., Comstock, J. M., et al.: Dominant role by vertical wind shear in regulating aerosol effects on deep convective clouds, J. Geophys. Res., 114, doi:10.1029/2009JD012352, 2009.

Fouquart, Y., and Bonnel, B.: Computation of solar heating of the Earth's atmosphere: a new parameterization, Beitr. Phys. Atmos., 53, 35-62, 1980.

Ha, K.-J., Nam, S., Jeong, J.-Y., et al., Observations utilizing Korean ocean research stations and their applications for process studies, Bull. Amer. Meteor. Soc., 100, 2061-2075, 2019.

Holben, B. N., Tanré, D., Smirnov, et al.: An emerging ground-based aerosol climatology: Aerosol optical depth from AERONET, J. Geophys. Res., 106, 12067–12097, 2001.

Houze, R. A., Cloud dynamics, Academic Press, 573 pp, 1993.

Hwang, S.-O., and Lee, D.-K.: A study on the relationship between heavy rainfalls and associated low-level jets in the Korean peninsula, J. Korean. Meteorol. Soc., 29, 133–146, 1993.

Jiang, H., Xue, H., Teller, A., Feingold, G., and Levin, Z.: Aerosol effects on the lifetime of shallow cumulus, Geophys. Res. Lett., 33, L14806, doi:10.1029/2006GL026024, 2006.

Kar, S. K., Lioi, Y.A., and Ha, K.-J. : Aerosol effects on the enhancement of cloud-to-ground lightning over major urban areas of South Korea, Atmos. Res. , 92, 80-87, 2009.

https://doi.org/10.5194/acp-2021-917
Preprint. Discussion started: 15 December 2021


Atmospheric Chemistry and Physics Discussions

952 Khain, A., BenMoshe, N., and Pokrovsky, A.: Factors determining the impact of aerosols
953 on surface precipitation from clouds: Attempt of classification, J. Atmos. Sci., 65,
954 1721-1748, 2008.
955 Khain, A., Pokrovsky, A., Rosenfeld, D., Blahak, U., and Ryzhkoy, A.: The role of CCN in
956 precipitation and hail in a mid-latitude storm as seen in simulations using a spectral
957 (bin) microphysics model in a 2D dynamic frame, Atmos. Res., 99, 129–146, 2011.
958 Khain, A., Rosenfeld, D., and Pokrovsky, A.: Aerosol impact on the dynamics and
959 microphysics of deep convective clouds, Quart. J. Roy. Meteor. Soc., 131, 2639-266,
960 2005.
961 Khain, A. D., BenMoshe, N., and A. Pokrovsky, A.: Factors determining the impact of
962 aerosols on surface precipitation from clouds: An attempt at classification, J. Atmos.
963 Sci., 65, 1721–1748, doi:10.1175/2007JAS2515.1, 2008.
964 Lebo, Z. J., and Morrison, H.: Dynamical effects of aerosol perturbations on simulated
965 idealized squall lines, Mon. Wea. Rev., 142, 991-1009, 2014.
966 Lee, D.-K., Kim, H.-R., and Hong, S.-Y.: Heavy rainfall over Korea during 1980–1990.
967 Korean, J. Atmos. Sci., 1, 32–50, 1998.
968 Lee, S., Ho, C.-H., Lee, Y. G., Choi, H.-J. and Song, C.-K.: Influence of transboundary air
969 pollutants from China on the high-PM10 episode in Seoul, Korea for the period
970 October 16−20, 2008. Atmos. Environ., 77, 430−439, 2013.
971 Lee, S. S., Donner, L. J., Phillips, V. T. J., and Ming, Y.: The dependence of aerosol effects
972 on clouds and precipitation on cloud-system organization, shear and stability, J.
973 Geophys. Res., 113, D16202, 2008.
974 Lee, S. S., Kim, B.-G., and Yum, S. S., et al.: Effect of aerosol on evaporation, freezing and
975 precipitation in a multiple cloud system, Clim. Dyn., 48, 1069-1087, 2016.
976 Lee, S. S., Li, Z., Mok, J., et al,: Interactions between aerosol absorption, thermodynamics,
977 dynamics, and microphysics and their impacts on clouds and precipitation in a
978 multiple-cloud system, Clim. Dyn., https://doi.org/10.1007/s00382-017-3552-x,
979 2017.
980 Lee, S. S., Kim, B.-G., Li, Z., Choi, Y.-S., Jung, C.-H., Um, J., Mok, J., and Seo, K.-H.:
981 Aerosol as a potential factor to control the increasing torrential rain events in urban
982 areas over the last decades, Atmos. Chem. Phys., 18, 12531–12550,

https://doi.org/10.5194/acp-2021-917
Preprint. Discussion started: 15 December 2021

Atmospheric Chemistry and Physics Discussions

https://doi.org/10.5194/acp-18-12531-2018, 2018.

Li, Z., Niu, F., Fan, J., Liu, Y., Rosenfeld, D., and Ding, Y.: Long-term impacts of aerosols on the vertical development of clouds and precipitation, Nat. Geosci., 4, 888-894, 2011.

Lu, Z., Zhang, Q., and Streets, D. G.: Sulfur dioxide and primary carbonaceous aerosol emissions in China and India, 1996–2010, Atmos. Chem. Phys., 11, 9839–9864, 2011.

Mlawer, E. J., Taubman, S. J., Brown, P. D., Iacono, M. J., and Clough, S. A.: RRTM, a validated correlated-k model for the longwave, J. Geophys. Res., 102, 16663-1668, 1997.

Morrison, H., and Grabowski, W. W.: Cloud-system resolving model simulations of aerosol indirect effects on tropical deep convection and its thermodynamic environment, Atmos. Chem. Phys., 11, 10503–10523, 2011.

Oh, H., Ha, K.-J. and Timmermann, A.: Disentangling Impacts of Dynamic and Thermodynamic Components on Late Summer Rainfall Anomailes in East Asia, J. Geophys. Res., 123, 8623-8633, 2018.

Oh, H.-R., Ho, C.-H., Kim, J., Chen, D., Lee, S., Choi, Y.-S., Chang, L.-S., and Song, C.-K.: Long-range transport of air pollutants originating in China: A possible major cause of multi-day high-PM10 episodes during cold season in Seoul, Korea. Atmos. Environ., 109, 23−30, 2015.

Pruppacher, H. R. and Klett, J. D.: Microphysics of clouds and precipitation, 714pp, D. Reidel, 1978.

Rosenfeld, D., Lohmann, U., Raga, G. B., et al.: Flood or drought, How do aerosols affect precipitation? Science, 321, 1309-1313, 2008.

Storer, R. L., van den Heever, S. C., and Stephens, G. L.: Modeling aerosol impacts on convection under differing storm environments, J. Atmos. Sci., 67, 3904-3915, 2010.

Seo, K.-H., Son, J. H., Lee, J.-H., and Park, H.-S.: Northern East Asian monsoon precipitation revealed by air mass variability and its prediction, J. Clim., 28, 6221-6233, 2013.

Tao, W.-K., Chen, J.-P., Li, Z., Wang, C., and Zhang, C.: Impact of aerosols on convective clouds and precipitation, Rev. Geophys., 50, RG2001, 2012.

Tao, W. K., Cloud resolving modeling, J. Meteorol. Soc. Jpn., 85B, 305–330,

https://doi.org/10.5194/acp-2021-917
Preprint. Discussion started: 15 December 2021

Atmospheric Chemistry and Physics Discussions

doi:10.2151/jmsj.85B.305, 2007.

van den Heever, S. C., Carrió, G. G., Cotton, W. R., DeMott, P. J., and Prenni, A. J.: Impacts of nucleating aerosol on Florida storms. part I: Mesoscale simulations, J. Atmos. Sci., 63, 1752–1775, 2006.

Wang, H., Skamarock, W. C., and Feingold, G.: Evaluation of scalar advection schemes in the Advanced Research WRF model using large-eddy simulations of aerosol-cloud interactions, Mon. Wea. Rev., 137, 2547-2558, 2009.

Weisman, M. L., and Klemp, J. B.: The dependence of numerically simulated convective storms on vertical wind shear and buoyancy, Mon. Wea. Rev., 110, 504-520, 1982.

https://doi.org/10.5194/acp-2021-917
Preprint. Discussion started: 15 December 2021


Atmospheric Chemistry and Physics Discussions

FIGURE CAPTIONS

Figure 1. Wind at 850 hPa level (m s^{-1}), equivalent potential temperature (K), and geopotential height (m) over Northeast Asia at (a) 21:00 LST December 23rd 2017 and (b) 09:00 LST July 27th 2015. Wind, equivalent potential temperature, and geopotential height are represented by arrows, a shaded field, and contours, respectively. The rectangle in the Korean Peninsula in (a) marks the Seoul area and that in the East-Asia continent in (b) marks the Beijing area.

Figure 2. Rectangles in (a) and (b) mark the Seoul area in the Korean Peninsula and the Beijing area in the East-Asia continent, respectively. A dot in (a) marks Baekryongdo island. In (a) and (b), the light blue represents the ocean and the green the land area.

Figure 3. Surface size distribution of aerosols (a) for the Seoul case and (b) for the Beijing case. Aerosol number concentration per unit volume of air is represented by N and aerosol diameter by D.

Figure 4. Time series of $PM_{2.5}$ observed at the ground station in Baekryongdo island (blue line) and of the average $PM_{2.5}$ over ground stations in the Seoul area (red line) between 07:00 LST on December 22nd and 21:00 LST on December 24th in 2017. Note that $PM_{2.5}$ observed at stations in the Seoul area is applied to the control-s run whose period is marked by the dashed rectangle. Time series of the average $PM_{2.5}$ over stations in the Seoul area in the low-aerosol-s run for the simulation period is also shown (black solid line).

Figure 5. Time series of precipitation rates at the surface, which are averaged over the domain and smoothed over 1 hour, (a) for the control-s and low-aerosol-s runs in the Seoul area and (b) for the control-b and low-aerosol-b runs in the Beijing area. In (a) and (b), the averaged and observed precipitation rates over the observation sites in the Seoul and Beijing areas, respectively, are also shown.

https://doi.org/10.5194/acp-2021-917
Preprint. Discussion started: 15 December 2021


Atmospheric Chemistry and Physics Discussions

Figure 6. Observed and simulated cumulative frequency distributions of precipitation rates at the surface for (a) the Seoul case, which are collected over the Seoul area, and (b) the Beijing case, which are collected over the Beijing area, at the last time step. Simulated distributions are in the control-s and low-aerosol-s runs for the Seoul case and in the control-b and low-aerosol-b runs for the Beijing case. The observed distribution is obtained by interpolating and extrapolating the observed precipitation rates to grid points and time steps in the control-s and control-b runs for the Seoul and Beijing cases, respectively.

Figure 7. Cumulative frequency distributions of the precipitation rates at the surface in the control-s and low-aerosol-s runs for the Seoul case at (a) 06:00, (b) 07:20, (c) 09:00, (d) 10:00 and (e) 12:00 LST.

Figure 8. Vertical distributions of differences in the area-averaged condensation, deposition and freezing rates, and cloud-liquid and snow mass density, and updraft mass fluxes between the control-s and low-aerosol-s runs at (a) 03:20, (b) 03:40, (c) 06:00 and (d) 12:00 LST.

Figure 9. Spatial distributions of terrain heights, column-averaged condensation rates and precipitation rates at the surface at (a) and (b) 03:40, (c) and (d) 06:20, (e) and (f) 07:20, (g) and (h) 08:00, (i) and (j) 08:20, (k) and (l) 08:40, (m) and (n) 09:00, (o) and (p) 10:00, (q) and (r) 10:20, (s) and (t) 11:00, (u) and (v)12:00, (w) and (x) 13:00, (y) and (z) 15:20 LST. The distributions in the control-s run are shown in (a), (c), (e), (g), (i), (k), (m), (o), (q), (s), (u), (w) and (y), and the distributions in the low-aerosol-s run are shown in (b), (d), (f), (h), (j), (l), (n), (p), (r), (t), (v), (x) and (z). Condensation rates are shaded. Dark-yellow and dark-red contours represent precipitation rates at 0.5 and 3.0 mm hr^{-1}, respectively, while beige, light brown and brown contours represent terrain heights at 100, 300 and 600 m, respectively. See text for yellow rectangles in (a), (b), (o) and (p)

Figure 10. Cumulative frequency distributions of the column-averaged condensation rates in the control-s and low-aerosol-s runs for the Seoul case at (a) 07:20 and (b) 09:00 LST.

https://doi.org/10.5194/acp-2021-917
Preprint. Discussion started: 15 December 2021


Atmospheric Chemistry and Physics Discussions

Figure 11. Cumulative frequency distributions of the precipitation rates at the surface in the control-b and low-aerosol-b runs for the Beijing case at (a) 16:00, (b) 17:00, (c) 17:20, and (d) 19:00 LST.

Figure 12. Vertical distributions of differences in the area-averaged condensation, deposition and freezing rates, and cloud-liquid and snow mass density, and updraft mass fluxes between the control-b and low-aerosol-b runs at (a) 14:20, (b) 15:40, (c) 16:00, (d) 17:20 and (e) 19:00 LST.

Figure 13. Spatial distributions of terrain heights, column-averaged condensation rates and precipitation rates at the surface at (a) and (b) 14:20, and (c) and (d) 17:20 LST. (a) and (c) are for the control-b run and (b) and (d) are for the low-aerosol-b run. Condensation rates are shaded. Dark-yellow and dark-red contours represent precipitation rates at 1.0 and 2.0 mm hr^{-1}, respectively, while beige, light brown, brown and dark brown contours represent terrain heights at 100, 500, 1000 and 1500 m, respectively. Yellow circles in (a) and (b) mark places where most of condensation occurs.

Figure 14. Cumulative frequency distributions of the column-averaged condensation rates in the control-b and low-aerosol-b runs for the Beijing case at (a) 17:20 and (b) 19:00 LST.

Figure 15. Mean precipitation rates corresponding to each column-averaged condensation rate for the control-b run. One standard deviation of precipitation rates is represented by a vertical bar at each condensation rate.

Figure 16. Spatial distributions of precipitation rates (shaded) and wind vectors (arrows) for the Beijing case at (a) and (b) 17:00, (c) and (d) 17:20, (e) and (f) 17:40, (g) and (h) 18:00, (i) and (j) 18:20, (k) and (l) 18:40, and (m) and (n) 19:00 LST. The distributions in the control-b run are in (a), (c), (e), (g), (i), (k) and (m). The distributions in the low-aerosol-b run are in (b), (d), (f), (h), (j), (l) and (n).

https://doi.org/10.5194/acp-2021-917
Preprint. Discussion started: 15 December 2021


Atmospheric Chemistry and Physics Discussions

Figure 17. Vertical distributions of (a) the area-averaged cloud-liquid and rain evaporation rates and (b) downdraft mass fluxes in the control-b and low-aerosol-b runs over a period from 17:00 to 19:00 LST.

Figure 18. Diagram that depicts the flux of the moist static energy (arrows) between area A (blue) and area B (red). See text for details.

https://doi.org/10.5194/acp-2021-917
Preprint. Discussion started: 15 December 2021

Atmospheric Chemistry and Physics Discussions

Simulations	Site	Concentrations of background aerosols acting as CCN
Control-s run	Seoul area	Observed and affected by the aerosol advection
Low-aerosol-s run	Seoul area	Same as those in the control-s run but unaffected by the aerosol advection
Control-b run	Beijing area	Observed
Low-aerosol-b run	Beijing area	Reduced by a factor of 3.1 as compared to those observed

Table 1. Summary of simulations

Simulations	The average flux of the moist static energy which crosses the boundary between areas A and B ($J\ m^{-2}\ s^{-1}$)	
	At 16:30 LST	16:30 to 17:00 LST
Control-b run	1.5×10^5	1.7×10^5
Low-aerosol-b run	1.1×10^5	1.2×10^5

Table 2. Average flux of the moist static energy which crosses the boundary between areas A and B at 16:30 LST and for a period from 16:30 to 17:00 LST.

https://doi.org/10.5194/acp-2021-917
Preprint. Discussion started: 15 December 2021

Atmospheric Chemistry and Physics Discussions

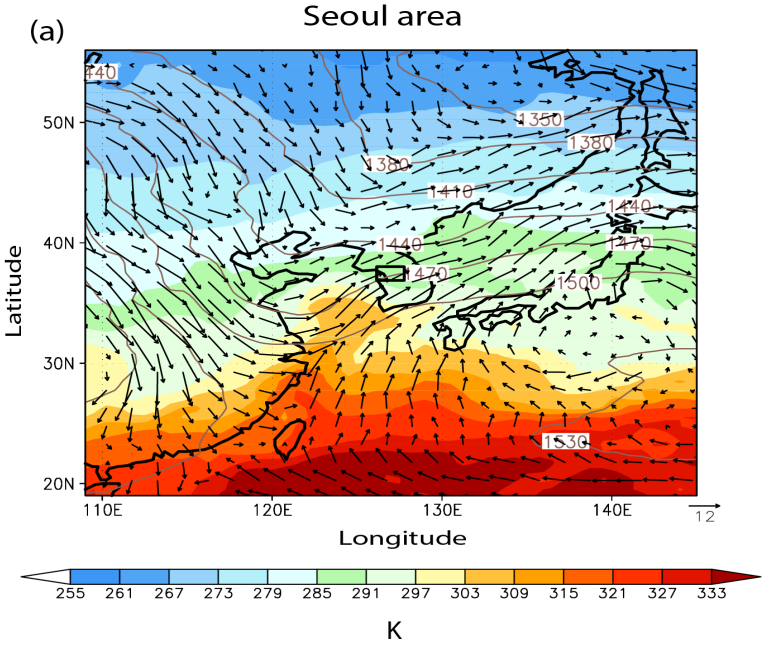

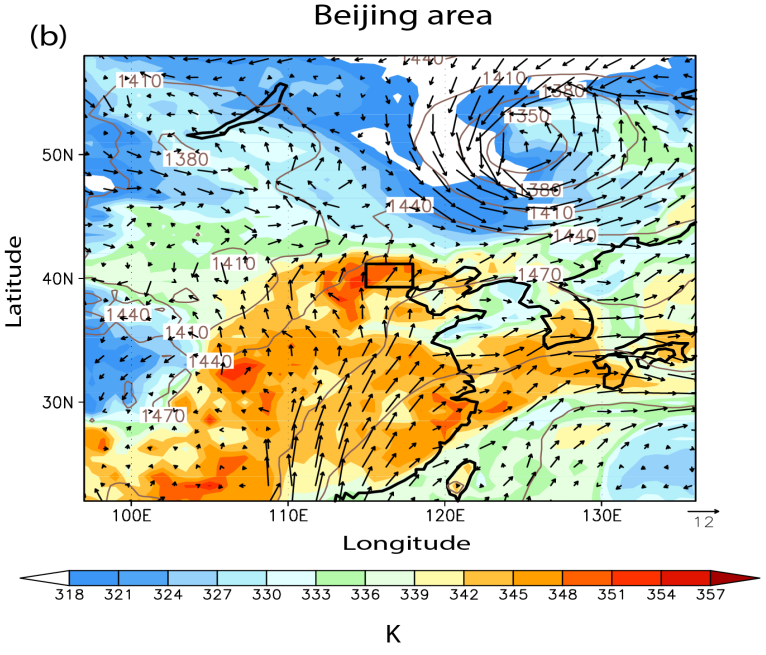

1189

1190 **Figure 1**

1191

https://doi.org/10.5194/acp-2021-917
Preprint. Discussion started: 15 December 2021

Atmospheric Chemistry and Physics Discussions

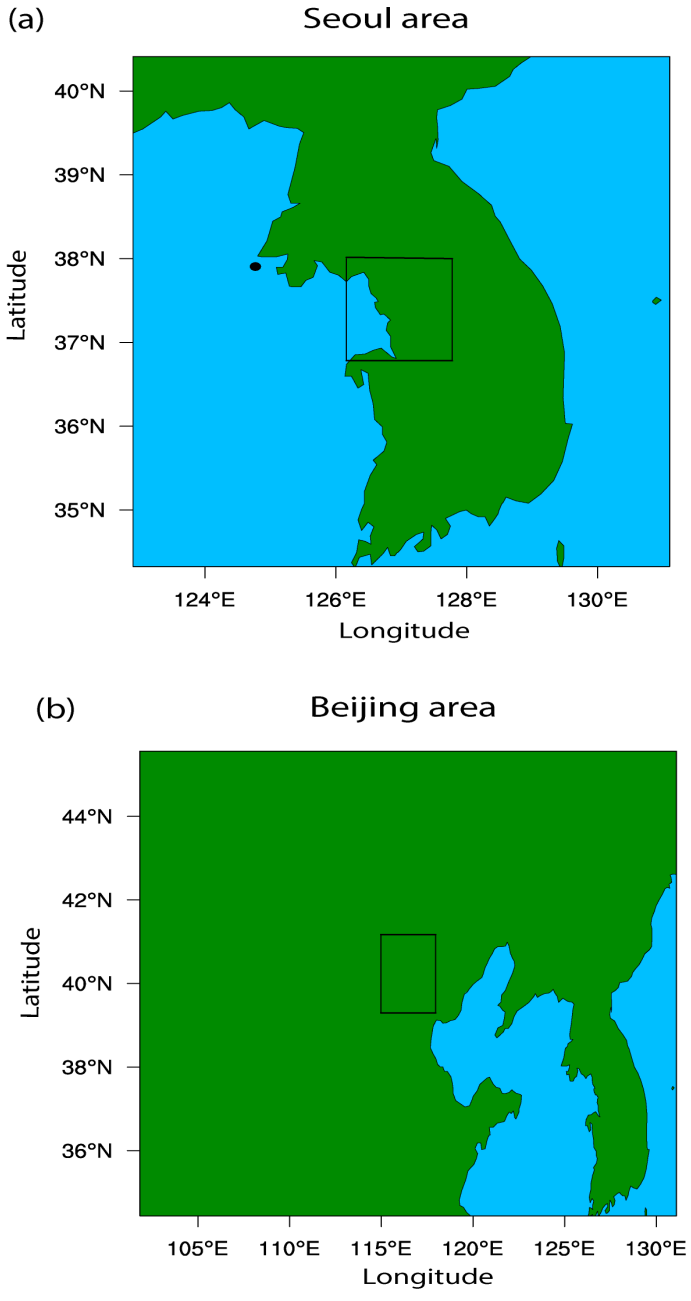

1192

1193 **Figure 2**

https://doi.org/10.5194/acp-2021-917
Preprint. Discussion started: 15 December 2021

Atmospheric Chemistry and Physics Discussions

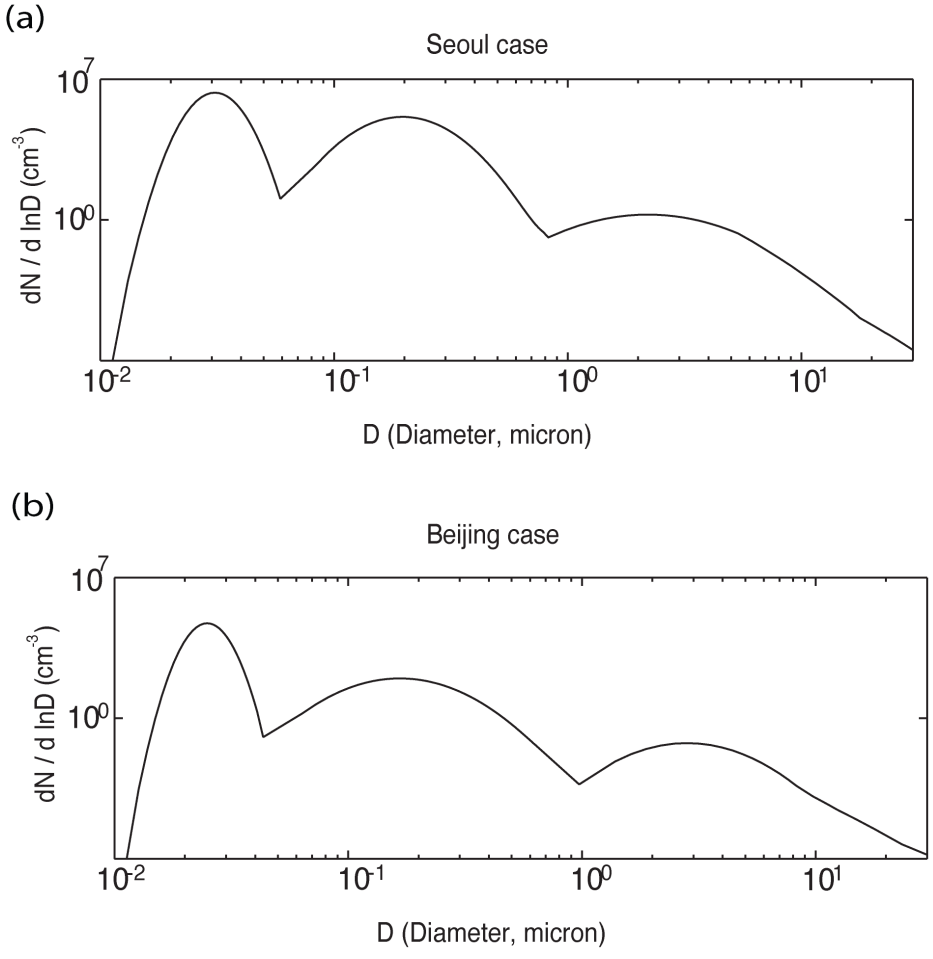

Figure 3

https://doi.org/10.5194/acp-2021-917
Preprint. Discussion started: 15 December 2021

Atmospheric Chemistry and Physics Discussions

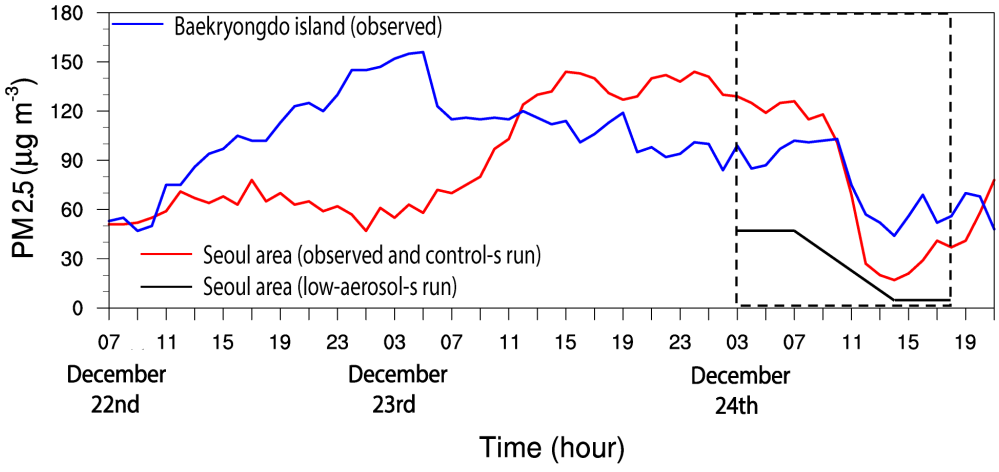

Figure 4

https://doi.org/10.5194/acp-2021-917
Preprint. Discussion started: 15 December 2021

Atmospheric Chemistry and Physics Discussions

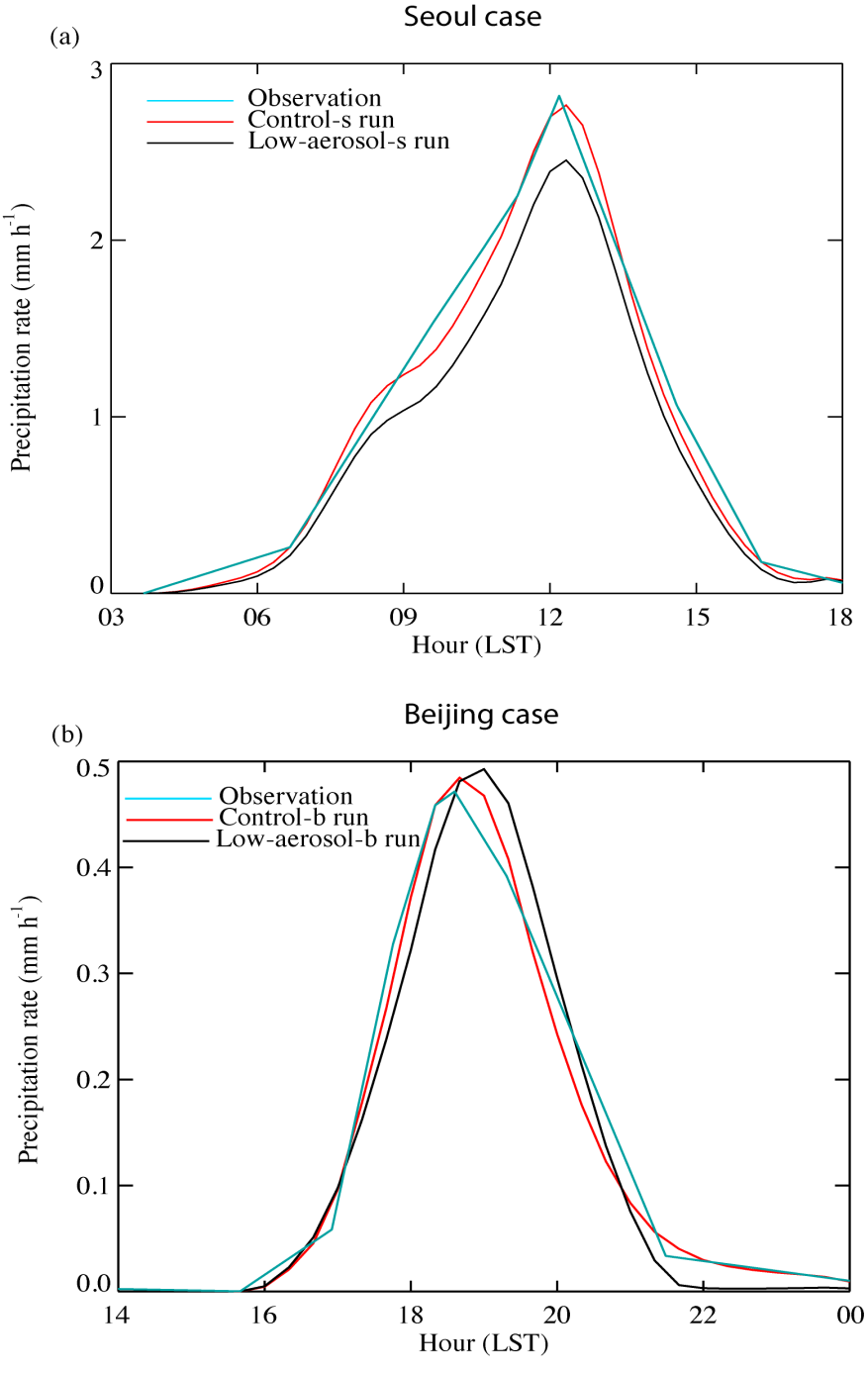

Figure 5

https://doi.org/10.5194/acp-2021-917
Preprint. Discussion started: 15 December 2021

Atmospheric Chemistry and Physics Discussions

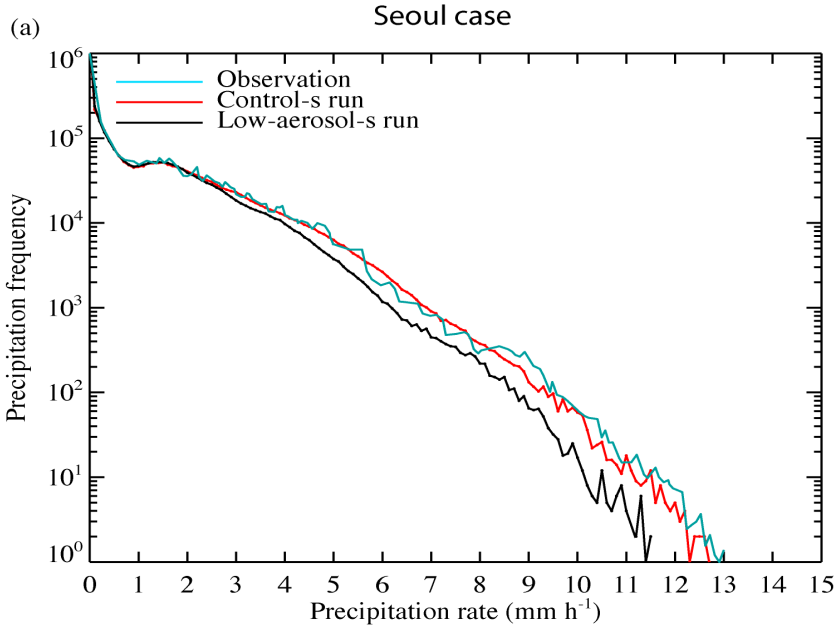

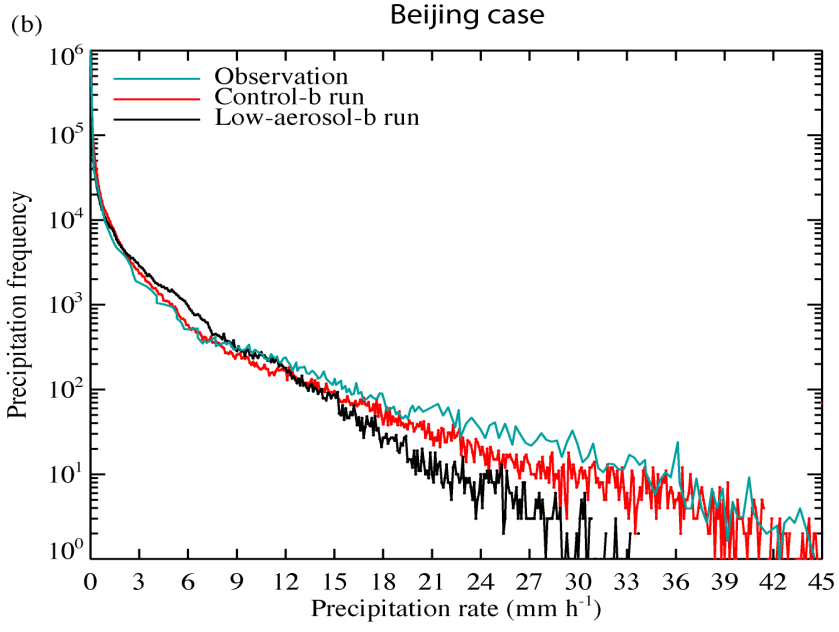

1215

1216 **Figure 6**

https://doi.org/10.5194/acp-2021-917
Preprint. Discussion started: 15 December 2021

Atmospheric Chemistry and Physics Discussions

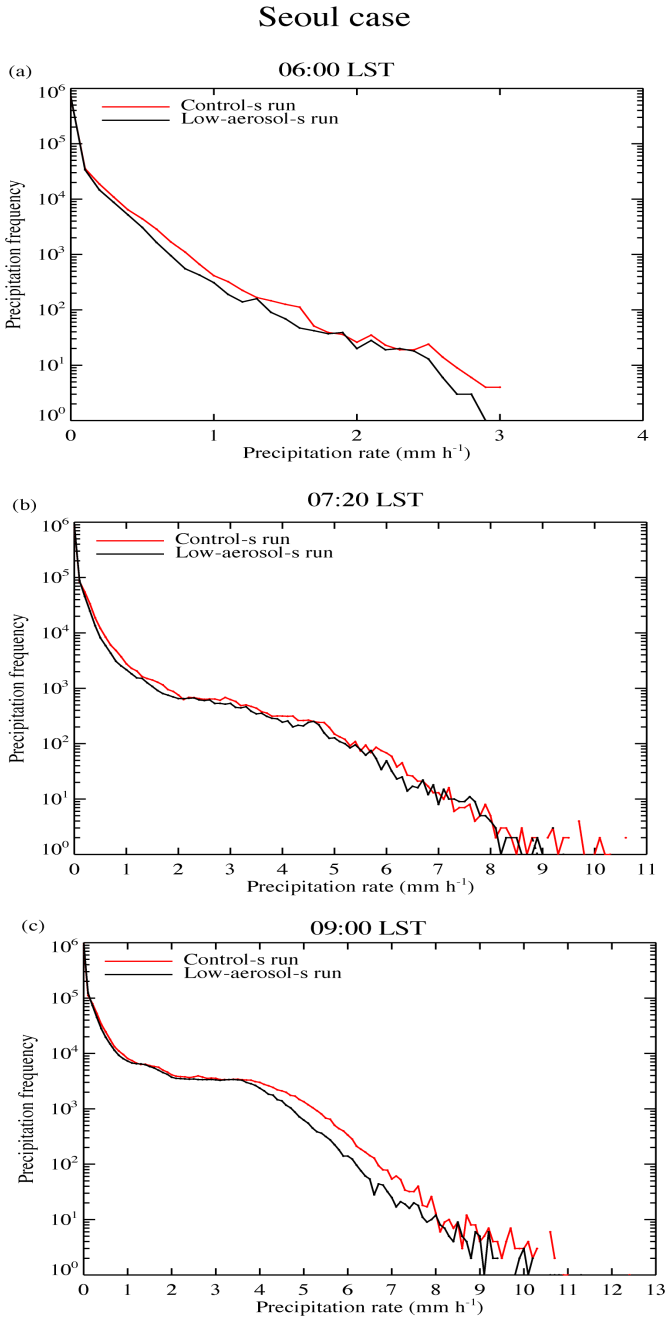

1217

1218 **Figure 7**

https://doi.org/10.5194/acp-2021-917
Preprint. Discussion started: 15 December 2021

Atmospheric Chemistry and Physics Discussions

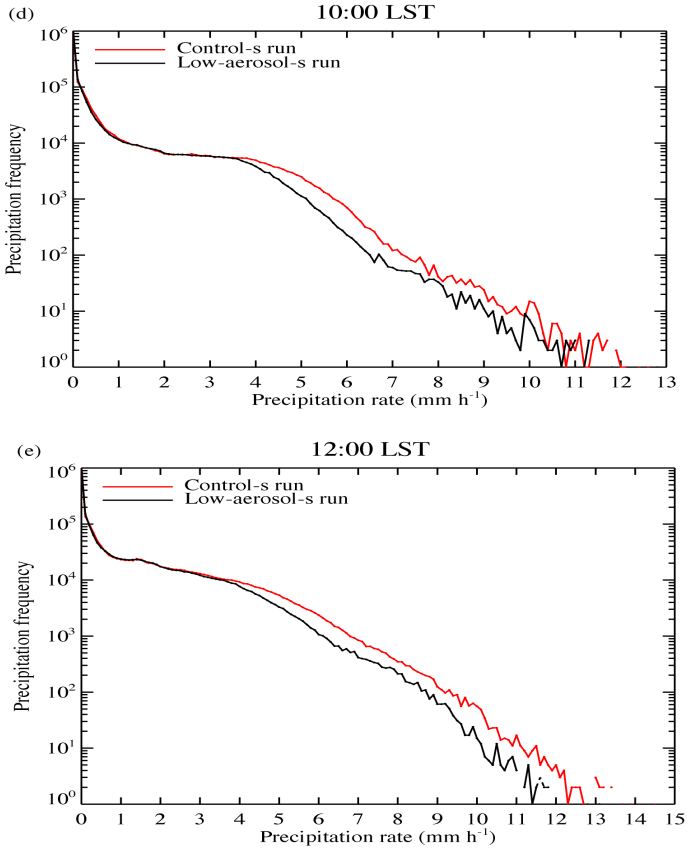

Figure 7

https://doi.org/10.5194/acp-2021-917
Preprint. Discussion started: 15 December 2021

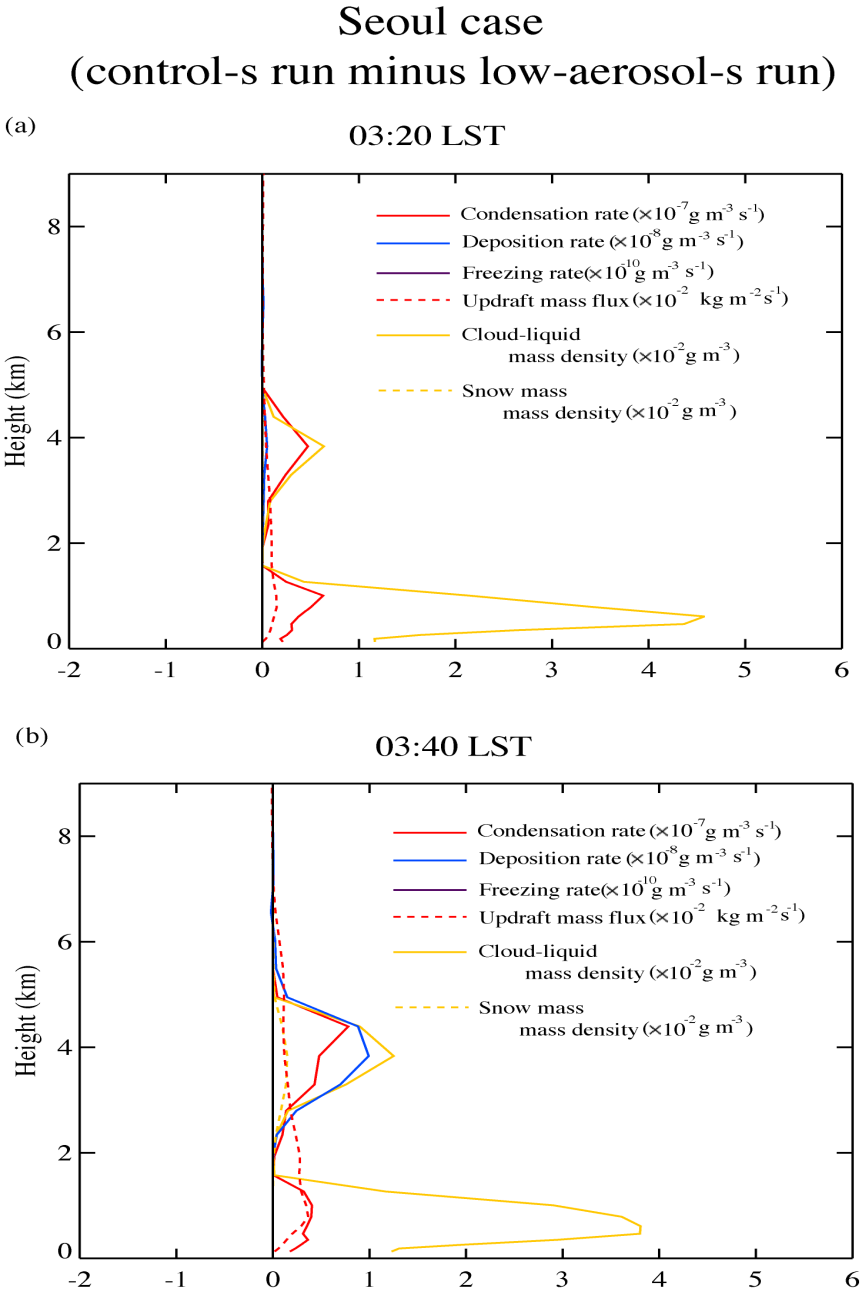

1227

1228 **Figure 8**

https://doi.org/10.5194/acp-2021-917
Preprint. Discussion started: 15 December 2021

Atmospheric Chemistry and Physics Discussions

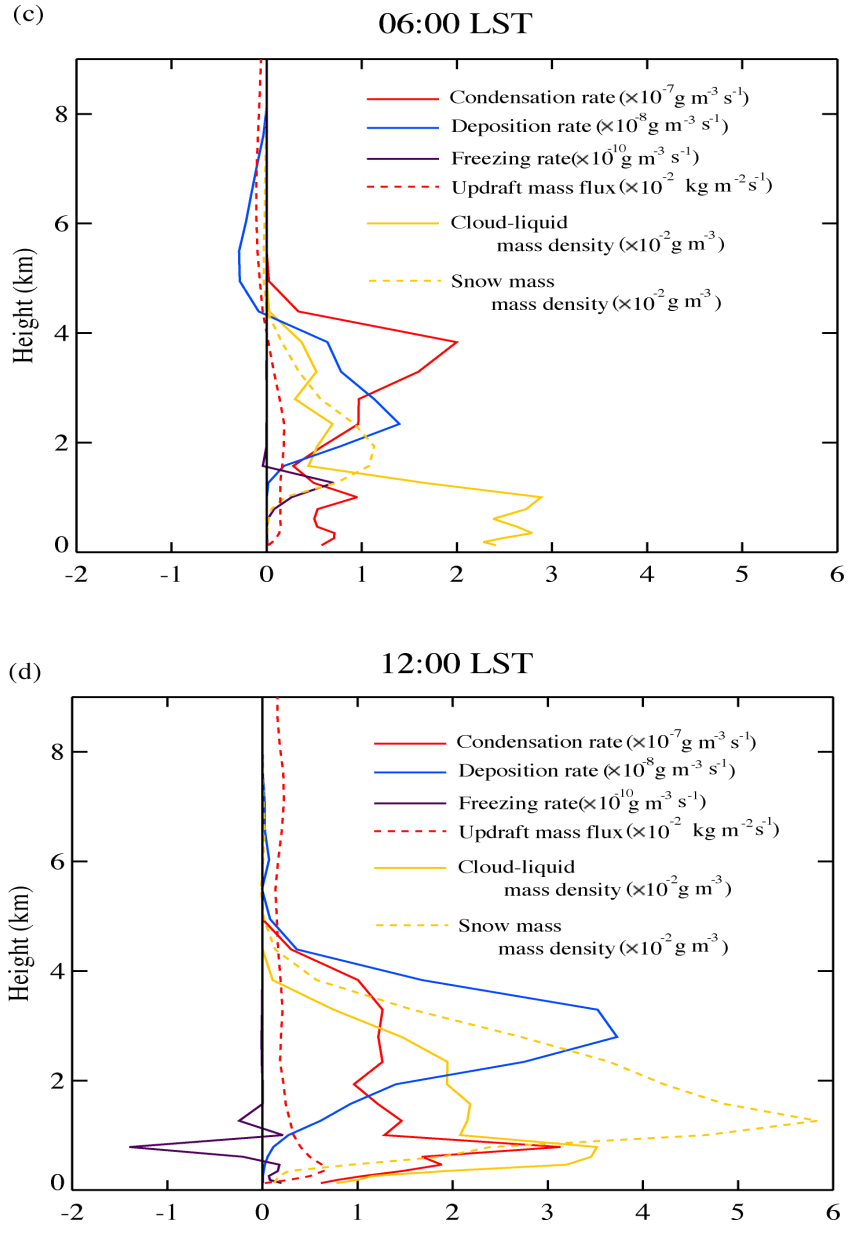

1229

1230 **Figure 8**

1231

https://doi.org/10.5194/acp-2021-917
Preprint. Discussion started: 15 December 2021

Atmospheric Chemistry and Physics Discussions

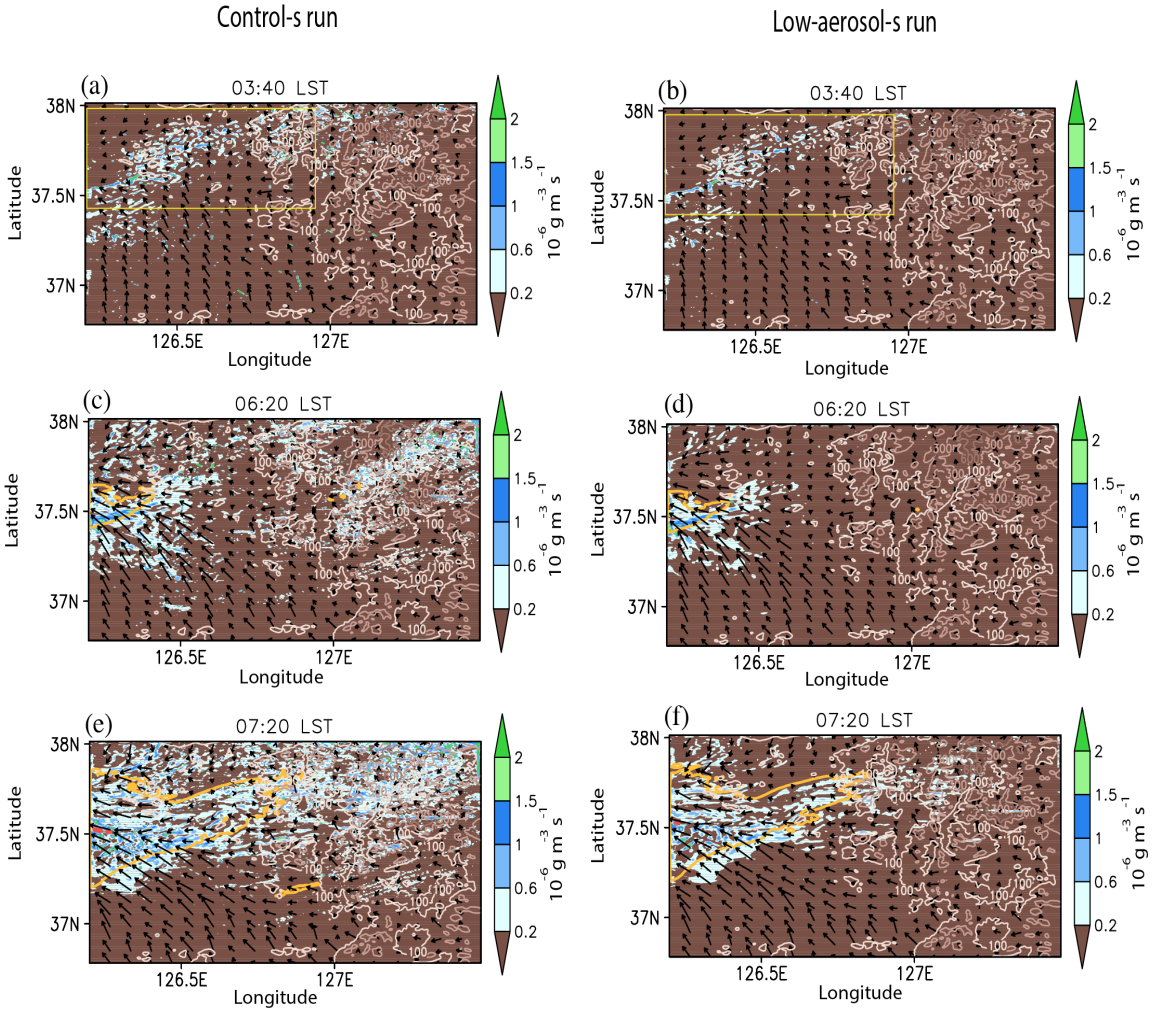

Figure 9

https://doi.org/10.5194/acp-2021-917
Preprint. Discussion started: 15 December 2021

Atmospheric Chemistry and Physics Discussions

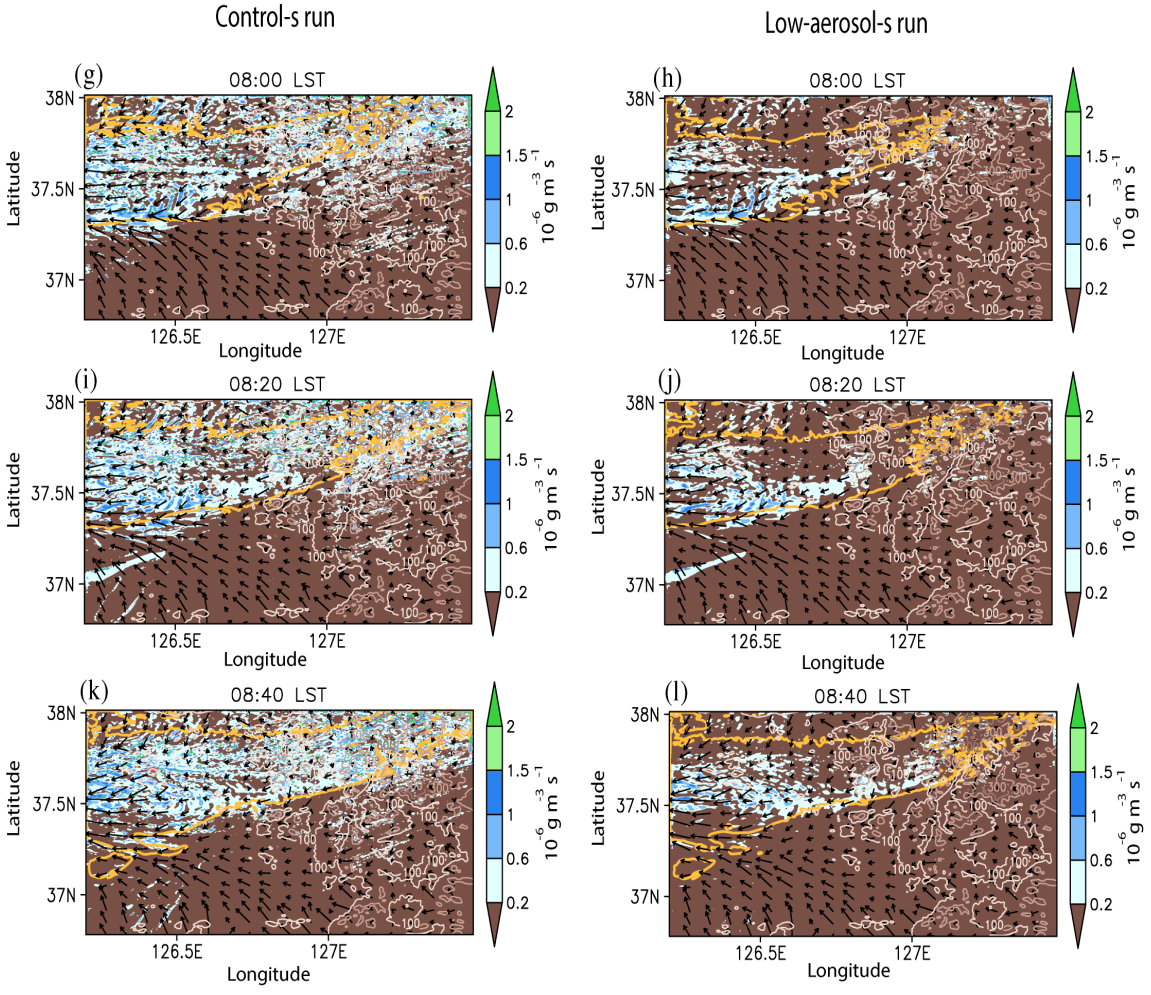

1238

1239 **Figure 9**

1240

1241

1242

1243

https://doi.org/10.5194/acp-2021-917
Preprint. Discussion started: 15 December 2021

Atmospheric Chemistry and Physics Discussions

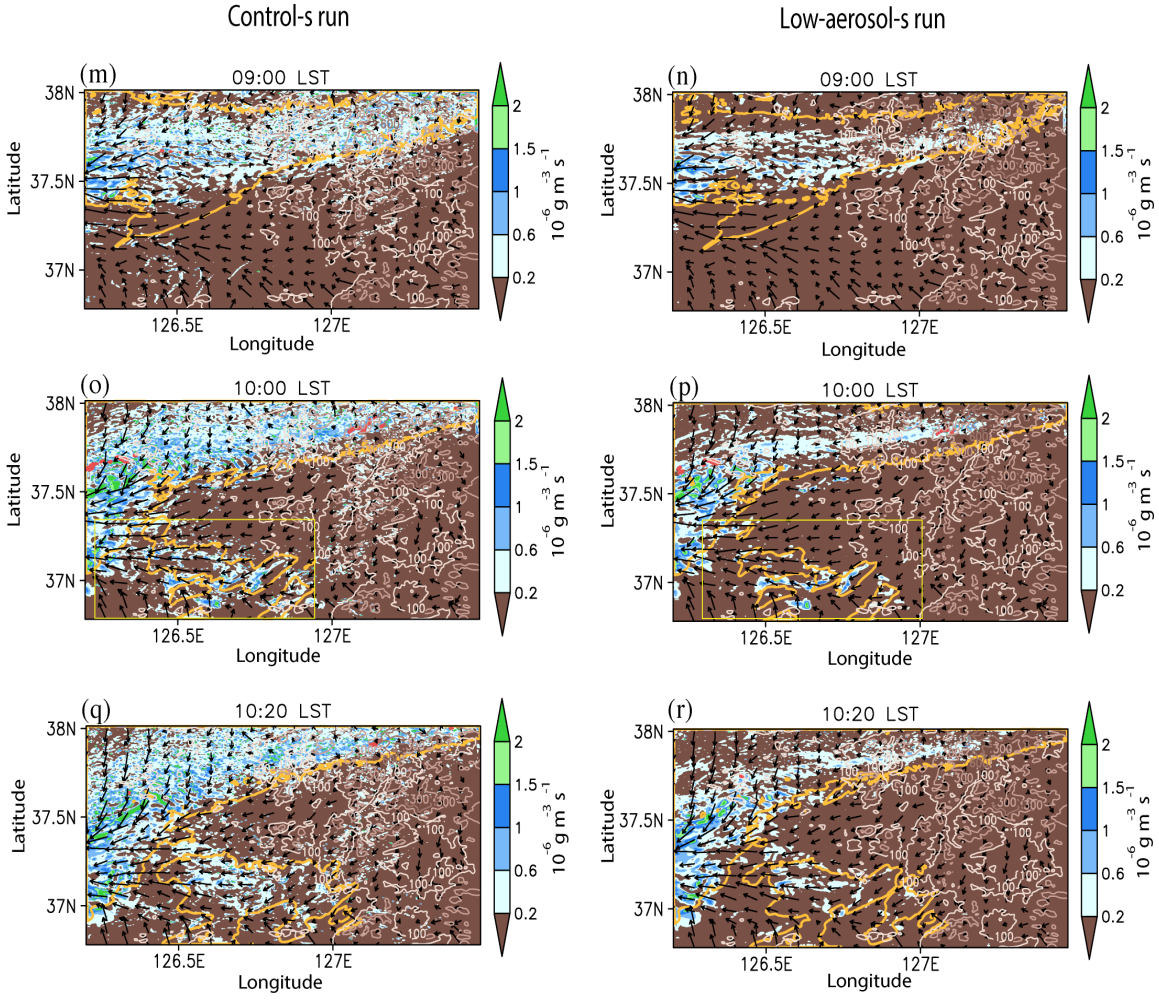

1244

1245 **Figure 9**

1246

1247

1248

1249

https://doi.org/10.5194/acp-2021-917
Preprint. Discussion started: 15 December 2021

Atmospheric Chemistry and Physics Discussions

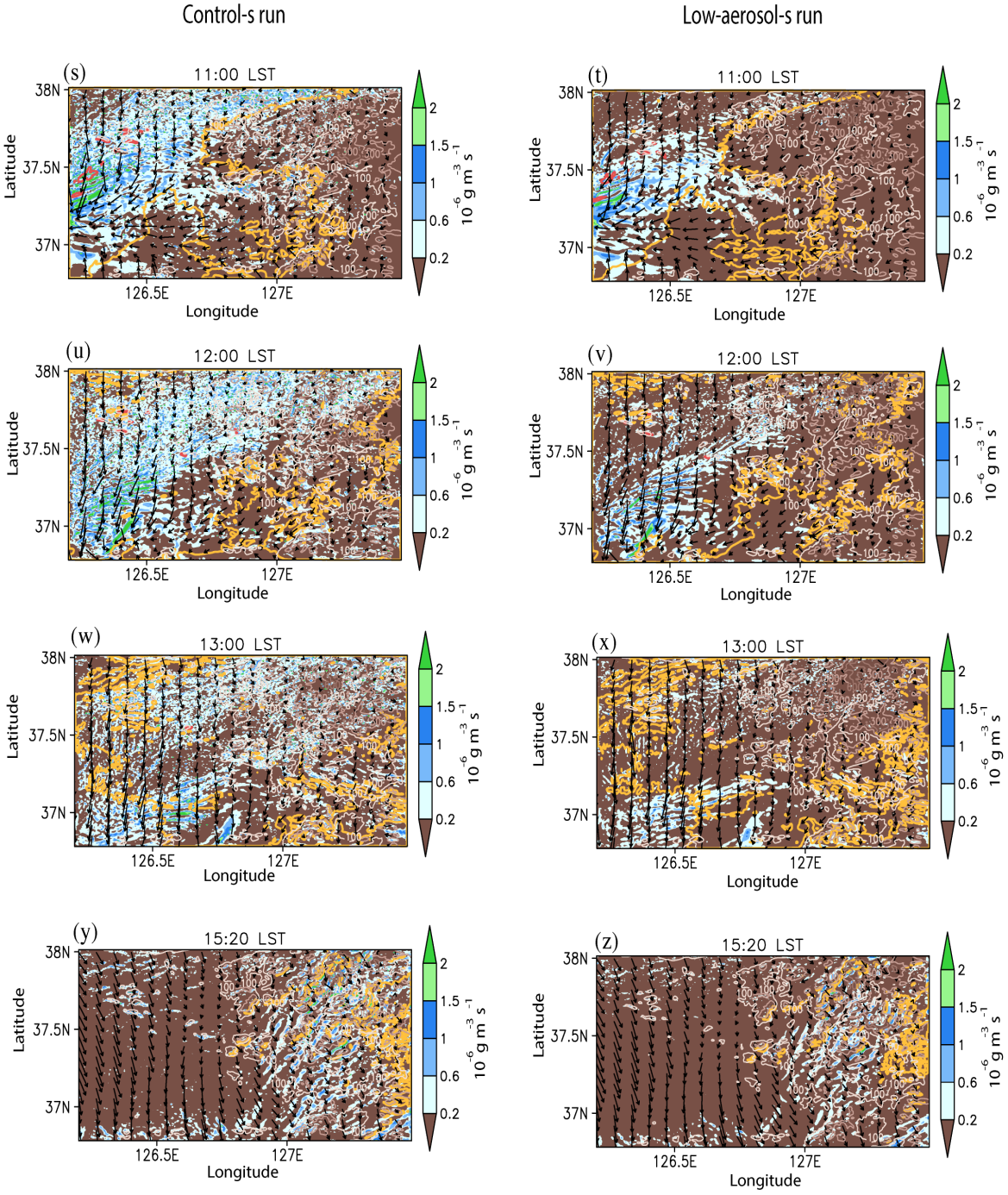

Figure 9

https://doi.org/10.5194/acp-2021-917
Preprint. Discussion started: 15 December 2021

Atmospheric Chemistry and Physics Discussions

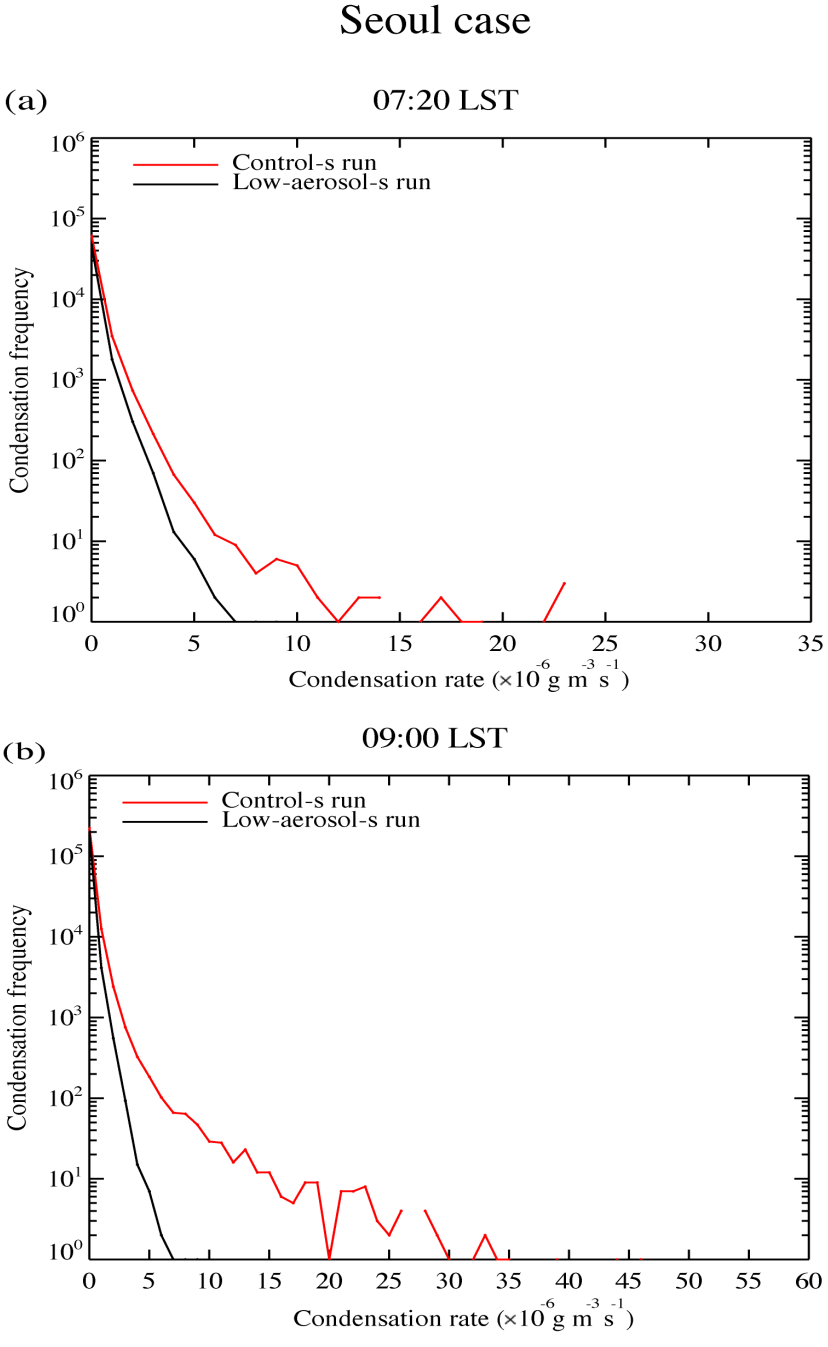

Figure 10

https://doi.org/10.5194/acp-2021-917
Preprint. Discussion started: 15 December 2021

Atmospheric Chemistry and Physics Discussions

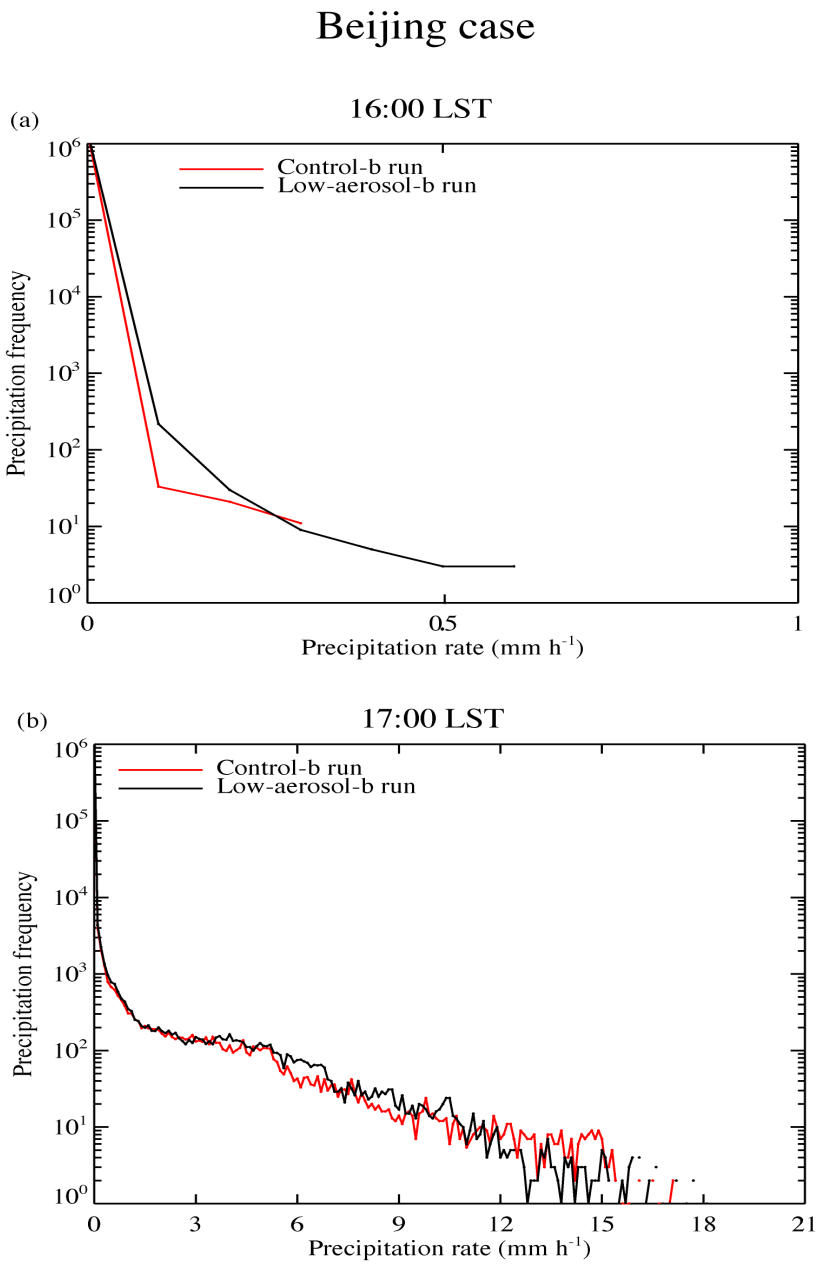

Figure 11

https://doi.org/10.5194/acp-2021-917
Preprint. Discussion started: 15 December 2021

Atmospheric Chemistry and Physics Discussions

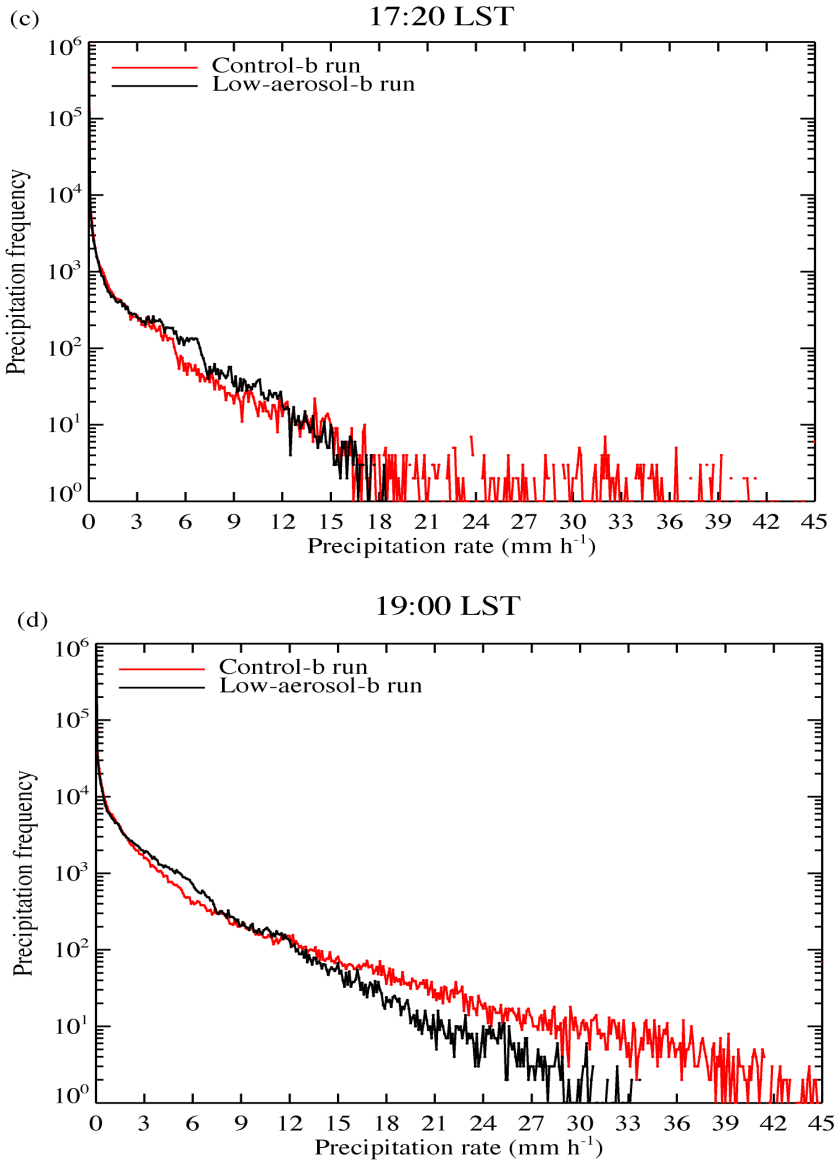

Figure 11

https://doi.org/10.5194/acp-2021-917
Preprint. Discussion started: 15 December 2021

Beijing case
(control-b run minus low-aerosol-b run)

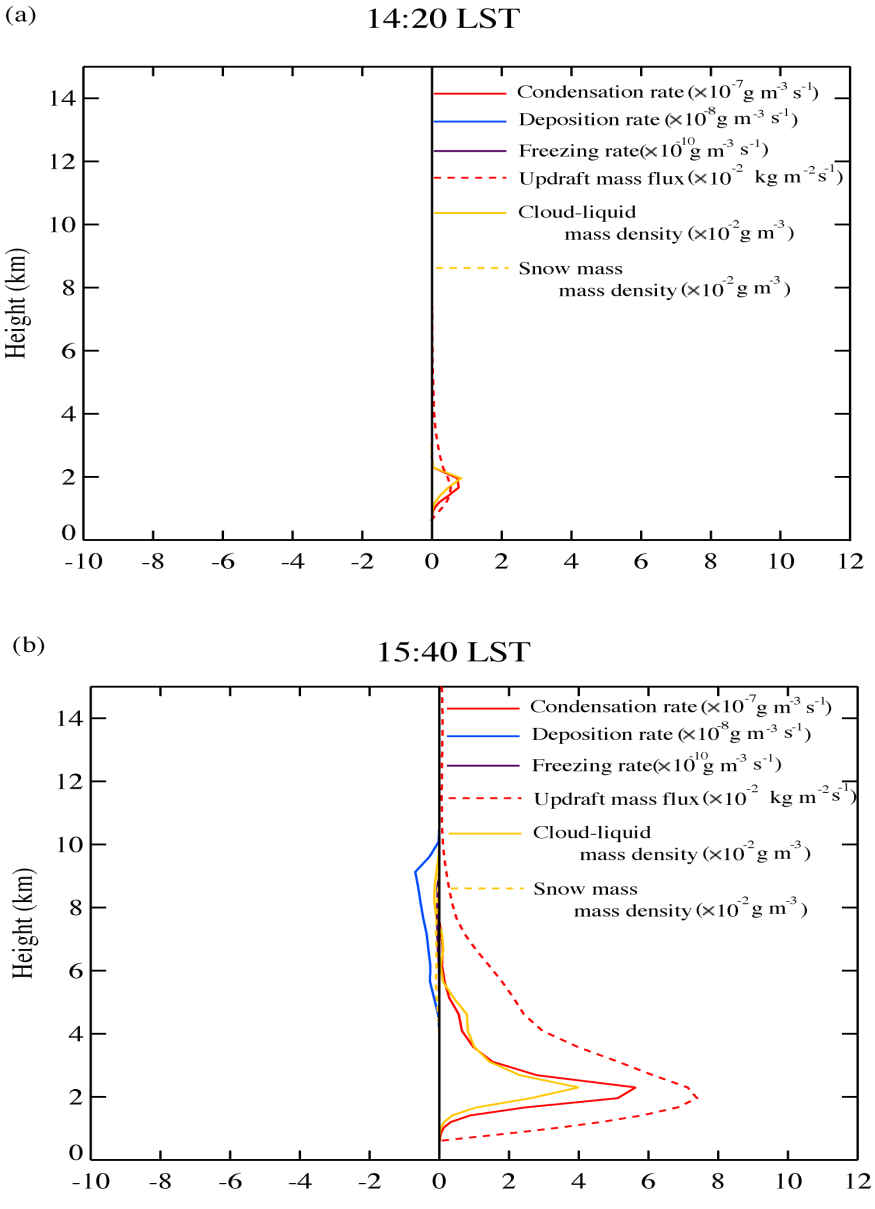

1264

1265 **Figure 12**

https://doi.org/10.5194/acp-2021-917
Preprint. Discussion started: 15 December 2021

Atmospheric Chemistry and Physics Discussions

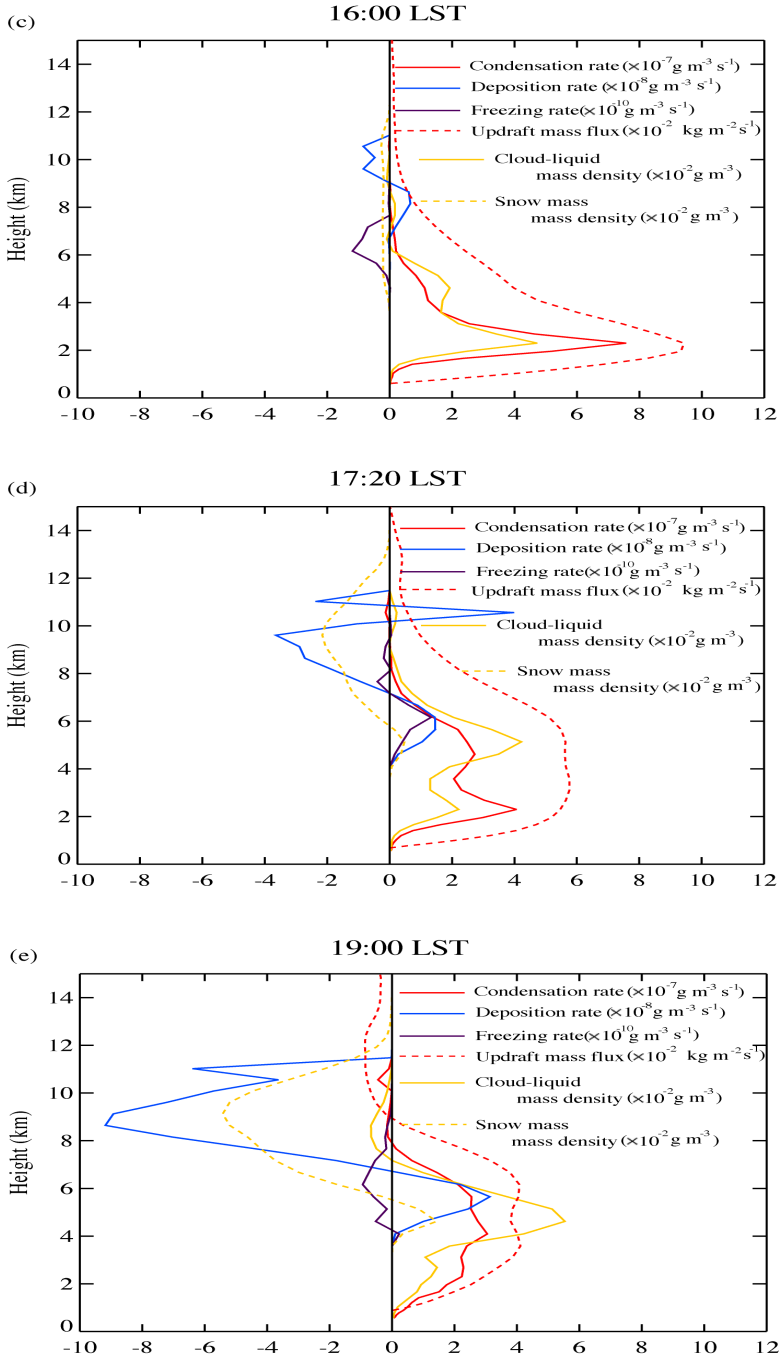

Figure 12

https://doi.org/10.5194/acp-2021-917
Preprint. Discussion started: 15 December 2021

Atmospheric Chemistry and Physics Discussions

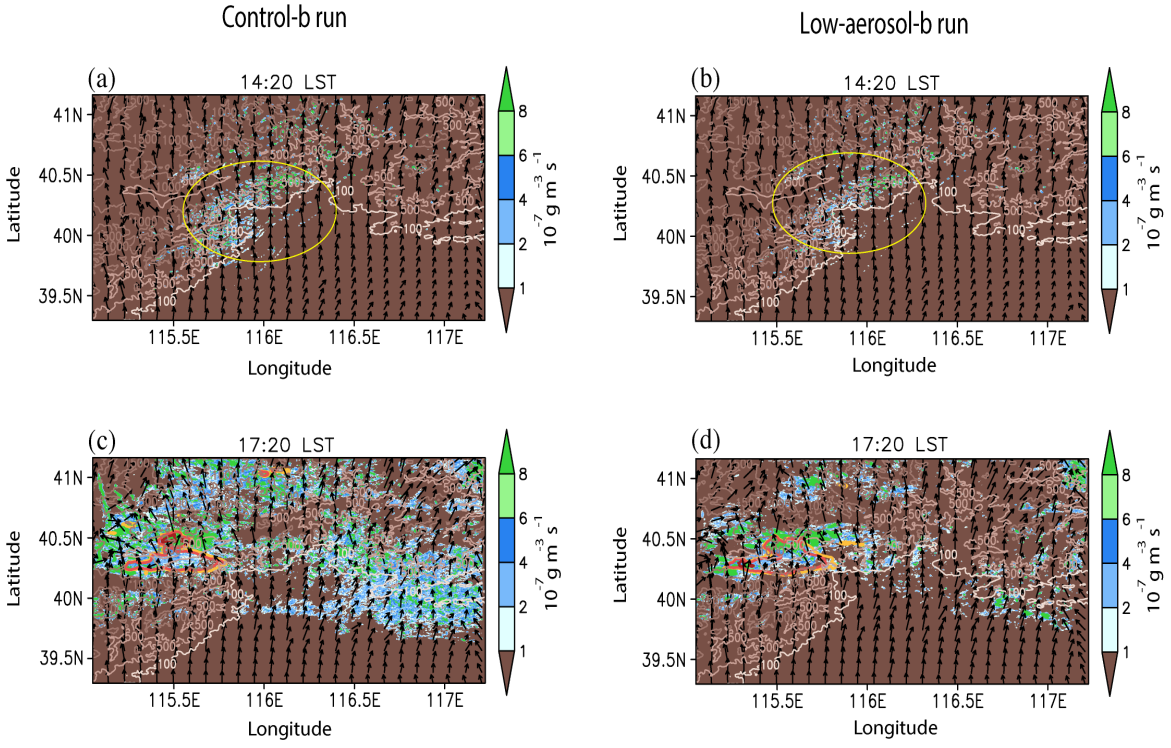

Figure 13

https://doi.org/10.5194/acp-2021-917
Preprint. Discussion started: 15 December 2021

Atmospheric Chemistry and Physics Discussions

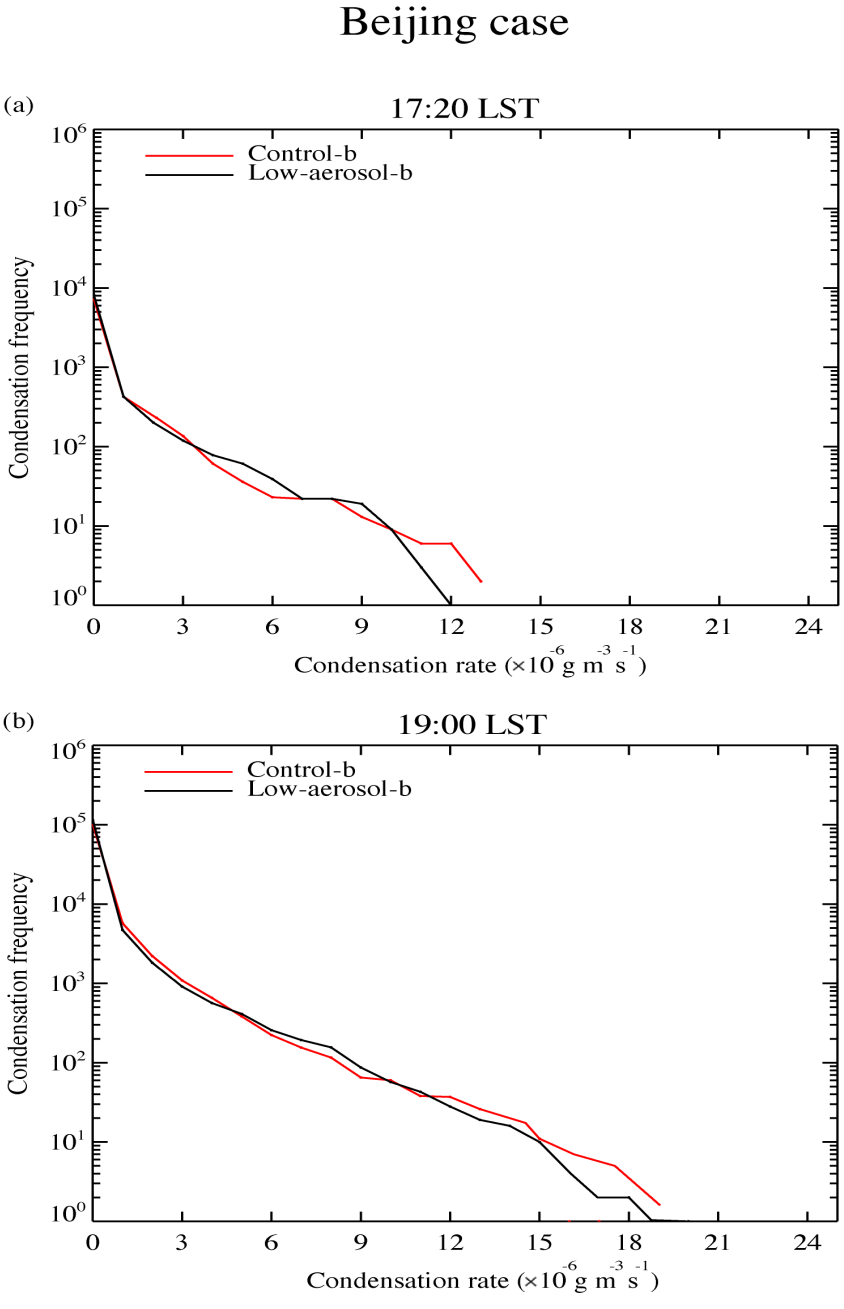

Figure 14

https://doi.org/10.5194/acp-2021-917
Preprint. Discussion started: 15 December 2021

Atmospheric Chemistry and Physics Discussions

1275

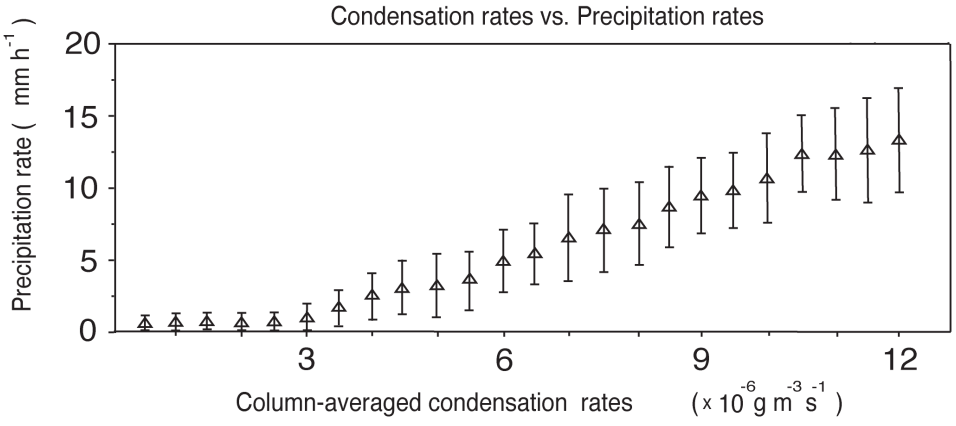

1276

1277 **Figure 15**

1278

1279

1280

1281

1282

1283

1284

1285

1286

1287

https://doi.org/10.5194/acp-2021-917
Preprint. Discussion started: 15 December 2021

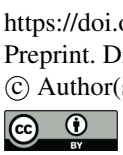

Atmospheric Chemistry and Physics Discussions

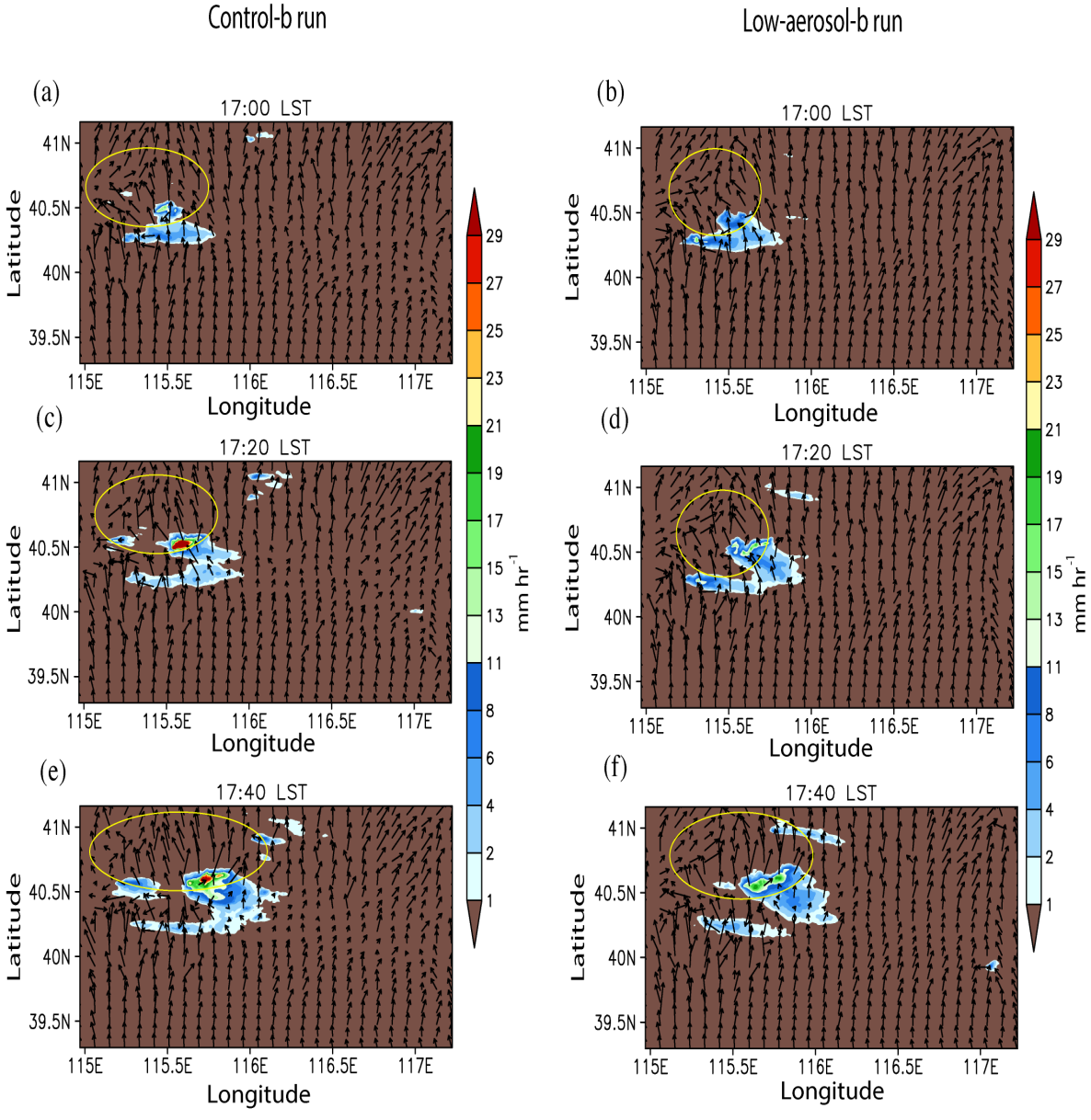

1288

1289 **Figure 16**

1290

https://doi.org/10.5194/acp-2021-917
Preprint. Discussion started: 15 December 2021

Atmospheric Chemistry and Physics Discussions

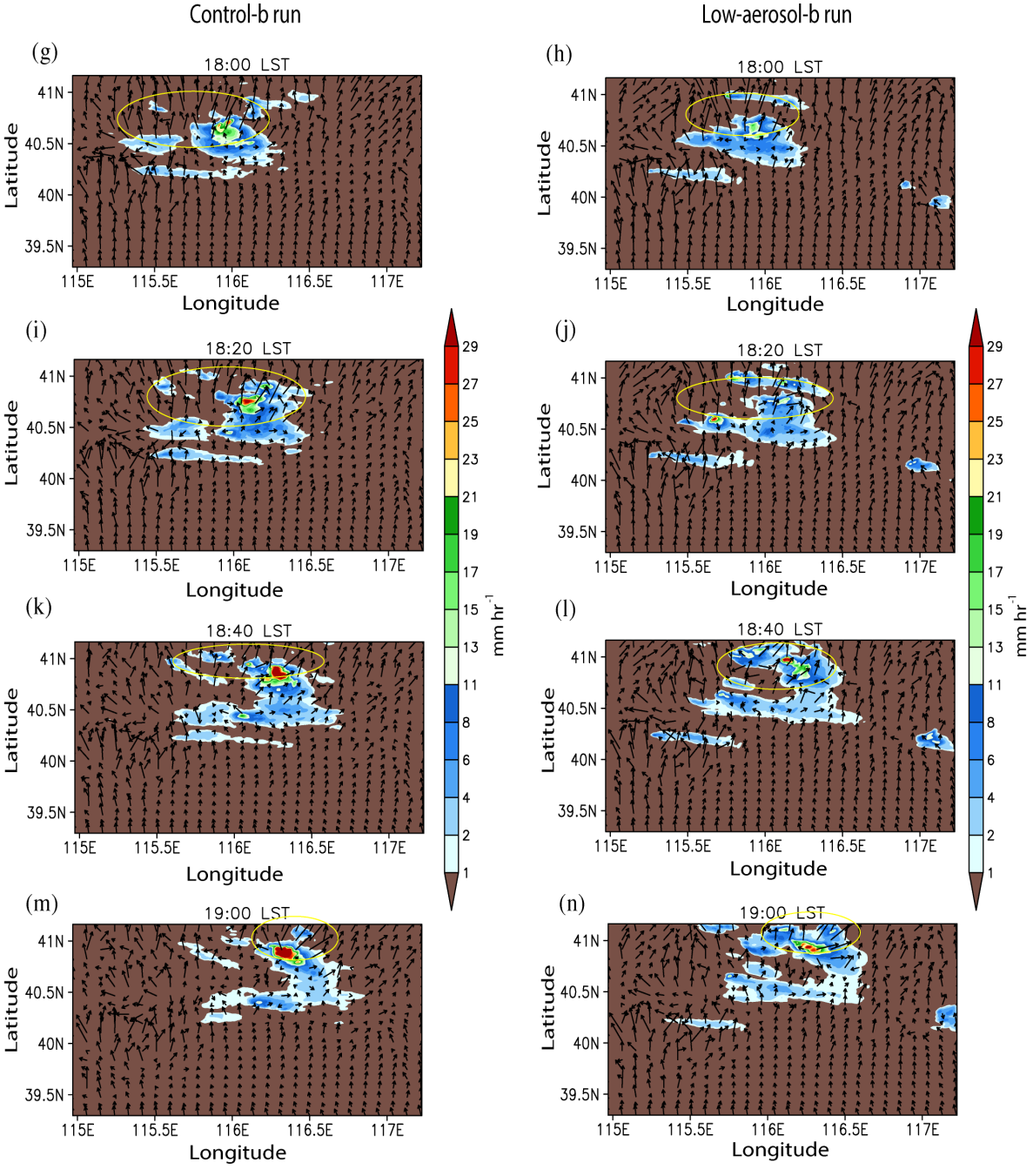

1291

1292 **Figure 16**

https://doi.org/10.5194/acp-2021-917
Preprint. Discussion started: 15 December 2021

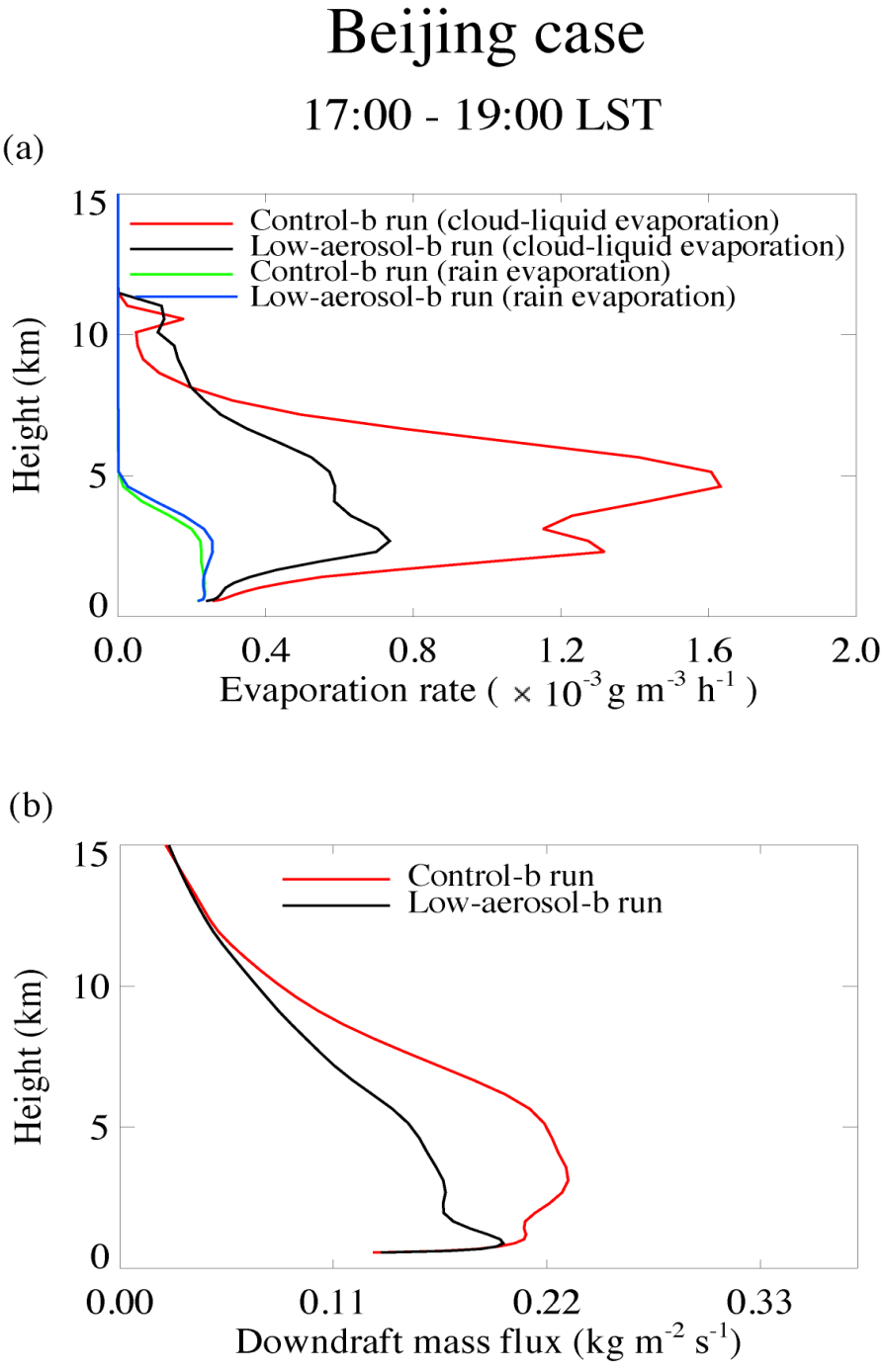

1293

1294 **Figure 17**

https://doi.org/10.5194/acp-2021-917
Preprint. Discussion started: 15 December 2021

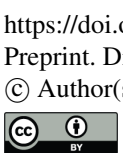

Atmospheric Chemistry and Physics Discussions

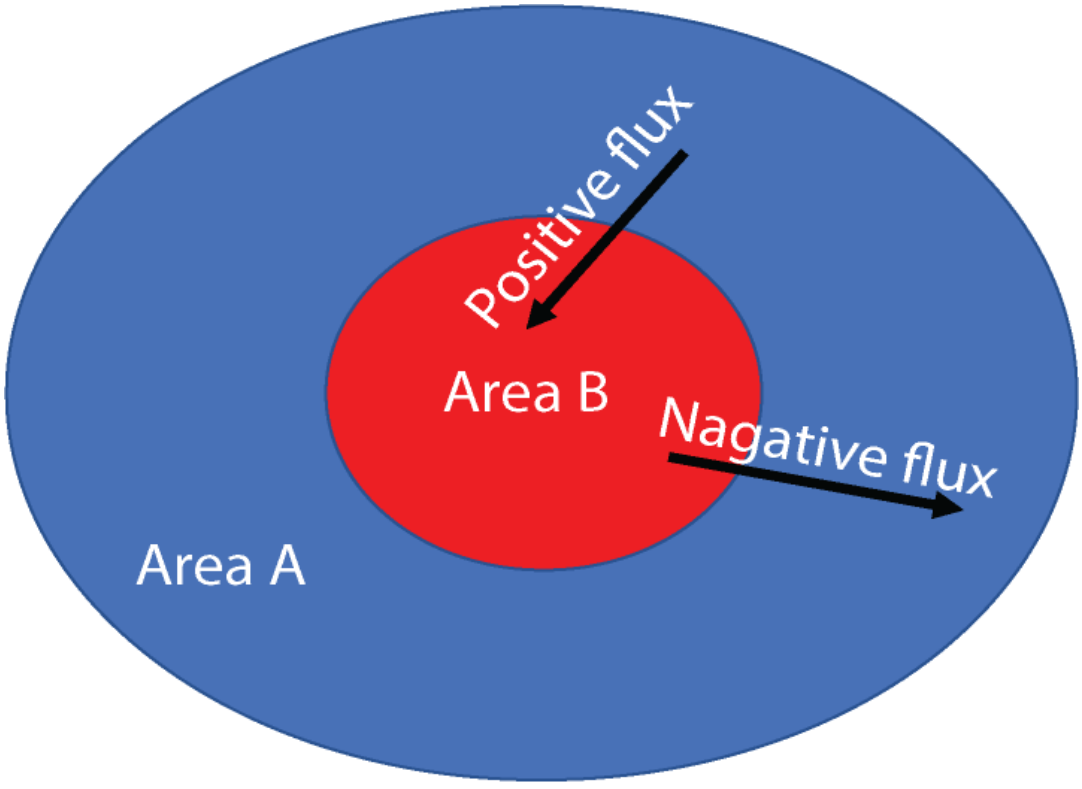

1295

1296 **Figure 18**

1297

1298

1299

1300

1301